UPPSALA
UNIVERSITET

UPTEC STS 21004
Examensarbete 30 hp
Januari 2021

Device Resonance Response in a Wave Energy Converter

Investigation of Surge Resonance in a Heaving Point Absorber

Lykke Östbom

UPPSALA
UNIVERSITET

Teknisk- naturvetenskaplig fakultet
UTH-enheten

Besöksadress:
Ångströmlaboratoriet
Lägerhyddsvägen 1
Hus 4, Plan 0

Postadress:
Box 536
751 21 Uppsala

Telefon:
018 – 471 30 03

Telefax:
018 – 471 30 00

Hemsida:
http://www.teknat.uu.se/student

Abstract

Device Resonance Response in a Wave Energy Converter

Lykke Östbom

Wave power possesses vast potential to become a considerable energy contributor. The main challenge for wave power to become competitive on the energy market is to minimize the delivered energy cost simultaneously as designing a wave energy converter (WEC) strong enough to survive extreme sea conditions. The Swedish company CorPower Ocean is developing a heaving WEC that converts the emerged relative heave motion to electricity. CorPower Ocean minimizes the delivered energy cost by letting the WEC resonate with the incoming wave providing maximization of the annual energy output. However, system characteristics of the WEC structure can produce resonance in other modes than heave which might affect the energy performance. This thesis targeted the device resonance response in CorPower Ocean's WEC in the surge mode. More specifically, the thesis investigated, through simulation, when resonance in surge occurs and whether the impacts of the resonance should be mitigated. The results indicated that the WEC is resonant in surge when the incident wave has a period between 6.5-10.5 s and 13.5-19 s. Moreover, the WEC is resonant in surge when the oscillation period in surge is 15-17 s. The surge resonance period and its bandwidth increase for higher wave loads. The surge resonance is negatively affecting the heave motion and the WEC's performance. It is not exactly known what in the structure that causes surge resonance. Two methods were used, results from one method showed tendencies that the mooring system was the instigator of the surge resonance, however, that could not be confirmed.

Handledare: Hannah Buckland
Ämnesgranskare: Jens Engström
Examinator: Elísabet Andrésdóttir
ISSN: 1650-8319, UPTEC STS 21004

Populärvetenskaplig sammanfattning

Vågkraft har stor potential att i framtiden bli en betydande energikälla. Om all världens utvinningsbara vågenergi som finns intill kuster utvanns skulle den energin stå för 75 % av dagens globala elektricitetsproduktion. Det är inte realistiskt att utvinna all den möjliga energin men endast en liten utvunnen del skulle göra vågkraft till en betydande energikälla. Vågkraft är en teknik som inte är fullt lika utvecklad som andra förnybara energitekniker som vindkraft och solkraft. För tillfället befinner sig vågkraftsindustrin i en demostreringsfas. Fullskaliga produkter finns men vågkraftsindustrin har fortfarande flera hinder att överkomma för att kunna etablera en mogen marknad med konkurrenskraftiga produkter. En av de stora utmaningarna är att ett vågkraftverk måste kunna hantera varierande vädersituationer, framförallt måste vågkraftverket vara starkt nog att stå emot stormvågor. Samtidigt som vågkraftverket måste vara robust nog att överleva stormar måste material- och underhållskostnaderna vara låga för att möjliggöra konkurrenskraftighet. Ett sätt möta denna utmaning är att minimera kostanden per levererad energienhet.

CorPower Ocean är ett svenskt företag som utvecklar en vågkraftsboj med ambitionen att ha kommersiell produkt 2023–2024. Principen bakom företagets vågkraftverk är att utvinna den relativa vertikala rörelsen som uppstår när en förtöjd boj flyter upp och ned med de förbipasserande vågorna. Den vertikala axeln för ett vågkraftverk kallas *heave.* För att minimera kostanden per levererad energienhet är bojen konstruerad att förstärka den uppkomna *heave*-rörelsen, således resonerar bojen med den inkommande vågen. En större relativ rörelse leder till mer producerad energi, följaktligen sänks kapitalkostnaden per levererad energienhet. Vågkraftsbojens systemegenskaper, vilka enbart är beroende av bojens struktur, kan emellertid ge upphov till naturlig resonans i andra riktningar än i *heave*. Att bojen resonerar i andra riktningar än den önskade *heave*-riktningen skulle eventuellt kunna minska bojens effektivitet att leverera energi. Ett vågkraftverk har sex frihetsgrader, vilket betyder att bojen kan röra sig i sex riktningar. Detta examensarbete syftade till att undersöka hur CorPower Oceans vågkraftsboj påverkas av resonans i *surge*, där *surge* är den axeln som representerar den horisontella riktningen en våg transporteras framåt i. *Heave* kan på svenska översättas till hävning, däremot finns det ingen vedertagen översättning av *surge*, av den anledningen behålls de engelska termerna i denna sammanfattning.

Surge-resonansen hos bojen undersöktes genom simulering. CorPower Ocean har utvecklat en modell som på ett tillförlitligt sätt beskriver bojens rörelse, således var simulering en god utgångspunkt för att uppfylla studiens syfte. Två olika metoder användes för att uppfylla arbetes syfte. Den första metoden, *”tvingad vågpåverkan”* (eng. ”forced oscillation”), begränsade bojen till att endast bli påverkad av den inkommande vågen i en riktning. Följaktligen kunde det besvaras vid vilka perioder bojen hade en förstärkt rörelse och befann sig i resonans i den tillåtna riktningen, exempelvis i *surge*. Den andra metoden bestod av att linjärisera vågkraftverket, då ett vågkraftverk är ett olinjärt system och det är svårt att finna systemegenskaper i ett

olinjärt system. Om ett olinjärt system linjäriseras kring en viss tidpunkt möjliggörs undersökning av systemegenskaperna kring den tidpunkten samt vad i strukturen som orsakar systemets resonans.

Studiens resultat från metoden av *”tvingad vågpåverkan”* tyder på att störst resonans i *surge* uppstår när bojen oscillerar i *surge* med en period av 15–17 s. Resonansperioden verkar vara beroende på kraften av den inkommande vågen, större kraft resulterar i högre resonansperiod. Studiens resultat tyder på den ovannämnda resonansperioden i *surge* uppstår när bojen träffas av vågor med perioder i intervallen 6.5–10.5 s och 13.5–19 s. Att bojen skulle träffas av vågor med en period större än 14 s är däremot inte troligt. Även dessa resonansperioder är beroende på storleken på den inkommande vågen, små vågor medför resonanstoppar vid lägre vågperioder och samt att resonansintervallen blir kortare för små vågor. Vidare tyder resultatet på att resonans i *surge* negativt påverkar *heave*-rörelsen och därmed påverkar vågkraftverkets prestanda. Resultatet från linjäriseringen visade tendenser på att resonansen har sitt upphov i förtöjningsstrukturen, dock gick inte detta att bekräfta. Känsligheten i att linjärisera ett dynamiskt system som ett vågkraftverk visade sig vara hög vilket medförde en ovisshet i resultatet. Avslutningsvis diskuterades den potentiella förmåga som linjäriseringsmetoden skulle kunna besitta i att peka ut vilka delar av strukturen som ger upphov till resonans. Diskussionen mynnade emellertid ut i att linjäriseringsmetoden är svår att utnyttja då metoden får en ”svart låda”-karaktär på grund av modellens höga komplexitet.

Sammanfattningsvis, *surge*-resonans verkar påverka prestandan i ett vågkraftverk som utnyttjar *heave*-rörelse. I CorPower Oceans vågkraftsboj uppstår resonans i *surge* när bojen oscillerar i *surge* med en period av 15–17 s. Denna resonans är mest framträdande när de inkommande vågorna har perioder mellan 6.5–10.5 s samt 13.5–19 s. *Surge*-rörelsen förstärks och resonansintervallen växer för inkommande vågor med högre kraft. Det är okänt vad i strukturen som ger upphov till resonansen, tendenser fanns på att förtöjningssystemet orsakar resonansen men detta kunde inte bekräftas.

Acknowledgments

This degree project within the exciting area of wave power would not have been possible without CorPower Ocean and I would like to thank CorPower Ocean for the opportunity of writing this thesis with you and for your warm and friendly welcome. A special thanks to my supervisor Hannah Buckland for your valuable guidance but also for showing me your inspirational way of working. Lastly, I would like to thank my subject reviewer Jens Engström at Uppsala University for your valuable insights guiding me to see the technology and the results from bigger perspectives.

Table of contents

Abbreviations, definitions, and nomenclature

Abbreviations

PTO	power take-off
RMS	root mean square
WEC	wave energy converter

Definitions

Heave	vertical direction of a wave, perpendicular to the propagation, see Figure 1.
Irregular wave	an irregular wave is a wave composed of several regular waves of different character.
Natural frequency	a natural frequency tends to be a resonance frequency when the system is subjected to an external force oscillating at the natural frequency. The natural frequency is solely dependent on the structure of the system.
Oscillation period	in this thesis an oscillation period is the period associated with an oscillatory motion in surge.
Regular wave	a regular wave can be described by a smooth sinusoidal, see Figure 1.
Resonance frequency	a resonance frequency is a frequency at which the system response is amplified when applying an external force oscillating at the resonance frequency. A resonance frequency is not necessarily a natural frequency.
Surge	horizontal and propagating direction of a wave, see Figure 1.
Wave period	in this thesis a wave period is the period associated with an oscillatory motion in heave, for instance the period of a sea wave.

Nomenclature

H	wave height [m], see Figure 1.
H_s	significant wave height [m], defined as the average value of the highest one-third heights of the incoming waves.
t	wave period [s], see Figure 1.
t_p	peak period [s], defined as the wave period a regular wave has when carrying the same amount of energy as the irregular one.
t_s	simulation time [s].

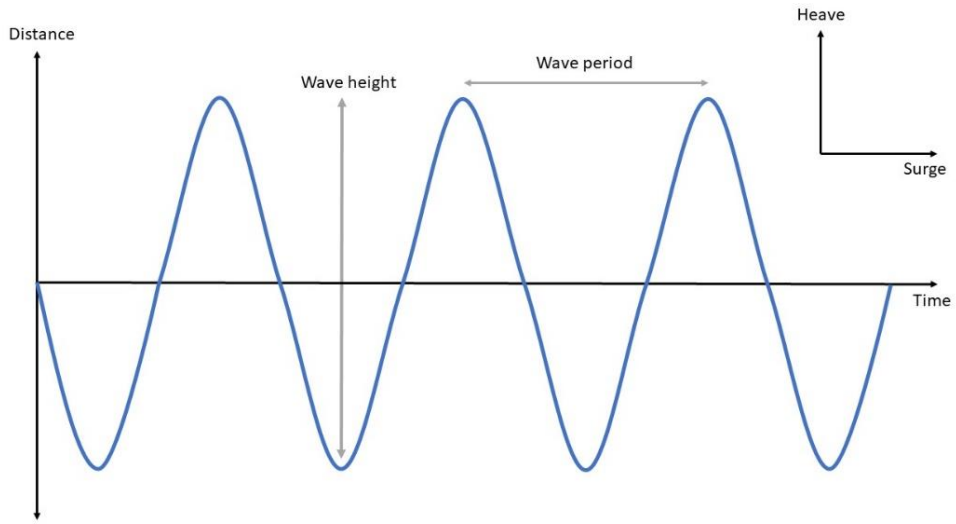

Figure 1. Illustration of a regular wave, wave height and wave period as well an illustration of the heave and surge modes in relation to the propagation of a wave.

1. Introduction

There is vast potential to extract energy from ocean waves. The extractable global wave power potential is estimated to be around 2.1 TW from waves incident the ocean-facing coastlines [1]. If all this potential power were to be harnessed it would provide nearly 75 % of the world's electricity consumption [2]. It is not realistic to extract all energy, nevertheless, only a small fraction harvested would make wave energy a considerable energy contributor. Moreover, the spatial energy density is substantially higher in waves compared to solar and wind energy [3]. Wave energy originates from solar energy via wind energy. Wave power is interesting from an energy production perspective since the energy gets more spatially concentrated in the generation from solar radiation to wind, and from wind to wave. However, wave power has not yet been utilized to its capacity, a consequence of highly dense energy is the challenge of managing increased loads without damaging the energy converter.

Wave power is not as a mature technology compared to other renewable technologies such as wind and solar. The extraction of wind and solar energy have successfully been deployed in a large commercial scale. Wave power is facing several technological challenges to become an equally significant energy producer. Sea states are geographically dependent and irregular in their nature, furthermore, sea states fluctuate hourly, daily, seasonally as well as yearly [3]. Therefore, wave energy converters (WECs) must be designed to operate under varying conditions and have a survivability that can cope with extreme sea states such as storms. In addition to operation in varying and harsh conditions, the delivered energy cost must be minimized for wave power to become a significant contributor to the world's energy supply [4]. The wave energy research has, during the last decades, evolved and made progress; wave power is in a demonstration phase where full scale trials, both dry tests and sea trials, are proceeded, however, wave power still faces challenges to become a competitive technology.

The delivered energy cost can be minimized by improving the power output performance of the WEC system. The performance can be increased through tuning the system to the local wave climate, i.e., designing the device to have a resonant frequency that coincides with the typical wave climate. A WEC in resonance with the incident wave will transfer more energy compared to a non-resonant device through increased amplitude and speed [5].

CorPower Ocean is a Swedish wave power company developing a WEC with the aim to successfully introduce a commercial product by 2023-2024 [6]. The concept behind CorPower Ocean's WEC is to utilize the relative heave motion a point absorber buoy floating on the sea surface experiences when anchored to the seabed via a tensioned mooring system [7]. A point absorber device is characterized by being much smaller than the incident wave's wavelength [8]. The waves' non-linear and irregular motion at the sea surface is converted into device response which later is transformed to

electricity. To maximize the energy absorption, CorPower Ocean's buoy is tuned to the wave climate to convert resonant device motion in heave. However, the characteristics of the WEC's structure can produce natural resonance in the surge mode when oscillating at the surge mode's natural frequency. This excitation might reduce the efficiency of the device and its ability to convert the relative heave motion into useful energy. This master thesis targets resonance in surge.

1.1 Purpose and research questions

The aim with this thesis is to investigate resonance responses in the surge mode in a point absorber type of WEC. The investigation are based on a case study and will look at when and how resonance in surge occurs in CorPower Ocean's WEC and whether the effects of the surge resonance should be mitigated. Further, if the effects should be mitigated, the thesis seeks to address how. The investigation is useful for improving the energy output performance of the WEC device.

To fulfil the aim of the thesis these research questions have been formulated:

- At what periods do surge resonance occur?
- How does resonance in surge affect the performance of the WEC?
- What instigates this resonance?

1.2 The field of research and motivations for the study

Wave energy is in its nature theoretically complex and most of the work on the subject has been simplified to some extent. A part of the wave power research that has not received a lot of attention is investigation of surge resonance in a WEC when the productive motion is associated with another mode. The productive mode in a point absorber WEC is generally heave, therefore, research in surge resonance is yet to a great extent undiscovered. An overview of the research field of point absorbers therefore results in mostly studies investigating heave resonance. For instance, [5] and [9] both studied, with a model restricted to the dominant motion in heave, how the frequency response in heave can be optimized by increasing the inertial mass with an additional submerged body. Moreover, [10] studied how the frequency response can be optimized by tuning the inertial mass through a tuning spring and additional rotational mass, and [11] tuned the frequency response through an external stiffness. The latter studies also utilized a model of the WEC restricted to the heave motion.

Nevertheless, there are a few studies investigating resonance characteristics for several modes through modal analysis. Modal analysis is the study of a dynamical system's frequency response associated with system characteristics. The modes' vibrational characteristics were studied in [12] to evaluate design choices of a three multi-mode (surge, heave, and pitch) submerged point absorber. In [13] modal analysis was utilized to investigate whether a coupled system of a heaving submerged spherical point absorber allowed to move in three directions (surge, heave, and pitch) would enhance

heave motion even when the buoy was excited in surge if the buoy had an asymmetric mass distribution. This thesis also considers a coupled system with multiple degrees of freedom; however, this thesis firstly examines the modal characteristics of the surge mode, and secondly, investigates whether the productive heave motion is affected.

Further, as mentioned in section 1. Introduction, wave power is yet an immature technology, the industry has not converged in a specific type of WEC leading to large variations in design. As opposed to the last two mentioned studies, CorPower Ocean's point absorber is floating and not submerged and as opposed to some of the previous mentioned studies, CorPower Ocean's design does not include an additional submerged body. The different technologies within the wave power industry will be mapped in section 2.3 Wave energy converter devices. Therefore, a case study can provide knowledge specific to a certain kind of system that not necessarily can be utilized for all design cases.

2. Background

The background section motivates and declares the general context around the study. The purpose of the background section is to describe the fundamental principles of WECs and to put CorPower Ocean's work in a bigger perspective. Lastly, the section is narrowed down to be more specific to the case of CorPower Ocean's WEC. A more theoretically context is presented which constitutes the theory that the methodology later is based upon.

2.1 CorPower Ocean

CorPower Ocean is a wave power company primarily based in Stockholm, Sweden. The company's technology is influenced by the pumping principle of the human heart and was first initiated 2009 and led to the company being founded in 2012 [14]. Since then, the company has gradually developed and tested the idea with increasing scales of physical prototypes and full-scale sea trials are expected to be proceeded in 2021. CorPower Ocean's goal is to successfully introduce WEC products in the market by 2023-2024 [6].

2.2 History of wave power and its resource

Today's work and research into renewable energy began in the oil crisis of the 1970's [15-16]. Renewable energy alternatives were seen more reliable compared to fossil fuel sources with their ties to geopolitics. The conflicts related to the crisis were eventually resolved and the balance on the oil market was restored, leading to a smaller focus on renewable energy. Since then, climate change has become one of the biggest issues of our time threatening the existence of the world with increased carbon emissions caused by the human [17]. As a result of the recognition of climate change, renewable energy

has been significant emphasized once again to mitigate the effects of the climate change by stabilizing the carbon emission in the energy sector [18]. Research within wave power has since the beginning of the 21st century gained more interest and made progress, today full-scale sea trials are being planned and proceeded as well as there are a few commercial products in the market [16].

As mentioned in 1. Introduction, wave energy is more spatially dense than solar and wind energy. The ratio between the three energy types is as follows; if a wave contains 2-3 kW/m^2 just below the sea surface, then solar radiation contains 0.1-0.3 kW/m^2 and wind 0.5 kW/m^2 [3]. The wave energy is located near the surface, there could be as much as 95 % of the energy located between the surface and one quarter of a wavelength below it [15]. Real sea waves are irregular in the sense that they cannot be mathematically described by a single frequency sinusoidal, however, irregular waves can be described by superposing several sine waves of different frequencies. As opposed to irregular waves, regular waves can be explained by a single sinusoidal and cannot illustrate an adequate sea wave, see Figure 2. In Figure 2 the irregular wave is a superposition of the two regular waves.

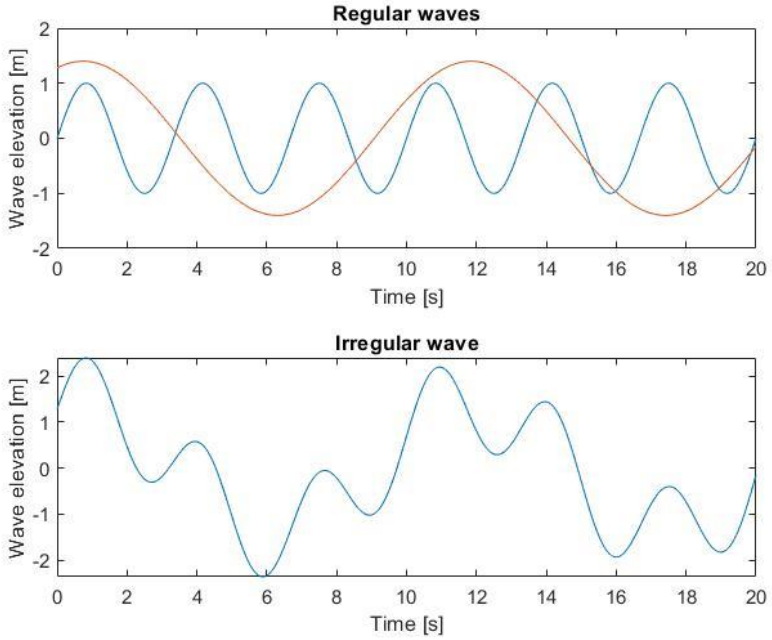

Figure 2. Illustration of regular and irregular waves. The irregular wave is a superposition of the two regular waves.

When a wave is propagating in a water depth exceeding one third of its wavelength, the wave is said to propagating in deep water and the seabed's influence on the wave may be neglected [3]. For irregular sea waves propagating in one direction, the average amount of stored energy [kJ/m^2] in a sea surface unit area is equal to [3]

$$E = \frac{\rho g H_s^2}{16} = \rho g \int_0^\infty S(f) df \quad (1)$$

where ρ is the density of water [kg/m^3], g the gravitational acceleration [m/s^2], and H_s the significant wave height for the sea state [m]. H_s is defined as the mean value of the highest one-third heights of the incoming waves. Nevertheless, the average amount of stored energy can also be explained as an integral over the wave spectrum $S(f)$ as in the right-hand side of equation (1), where f denotes frequency. A wave spectrum demonstrates how different frequencies of a wave contribute to the wave energy and it is represented in the unit [m^2/Hz]. f is the frequency a regular wave with the same amount of energy has. Analogously, the peak period t_p is defined as the wave period a regular wave has when carrying the same amount of energy as the irregular one. As a result, the wave elevation can be derived from the wave spectrum. Figure 3 illustrates the JONSWAP spectrum for $t_p = 11\ s$ for three different wave heights. JONSWAP is an abbreviation of Joint North Sea Wave Observation Projects that was a research project in the 1970's calculating the wave spectrum for a sea state that is not fully developed. A not fully developed sea state is dependent on both the wind speed and the fetch length [19]. In contrast, a fully developed sea state requires that the wind has blown across a sufficiently large area of the sea for a sufficiently long time, causing the wind and wave to be in equilibrium with each other and is only dependent on the wind speed [19]. The JONSWAP spectrum is suitable for sea states where CorPower Ocean's WEC will be deployed. CorPower Ocean will in 2021 install their WEC in Aguçadoura, Portugal, and the company are globally looking for other sites of interest. The WEC is planned to be deployed at a water depth of 45 m. The occurrence of a sea state in shallow waters is dependent on the water depth [20]. [20] has mapped the probability of various sea states at different water depth at the Aguçadoura site. The most typical sea states at the water depths of 20 m and 58 m are characterized by peak periods in the interval $t_p = 8 - 11.5\ s$ and significant wave heights in the interval $H_s = 1 - 3\ m$. In general, it is unlikely that $t_p \geq 14\ s$, for these two water depths the probability that $t_p \geq 14\ s$ is less than 6 %.

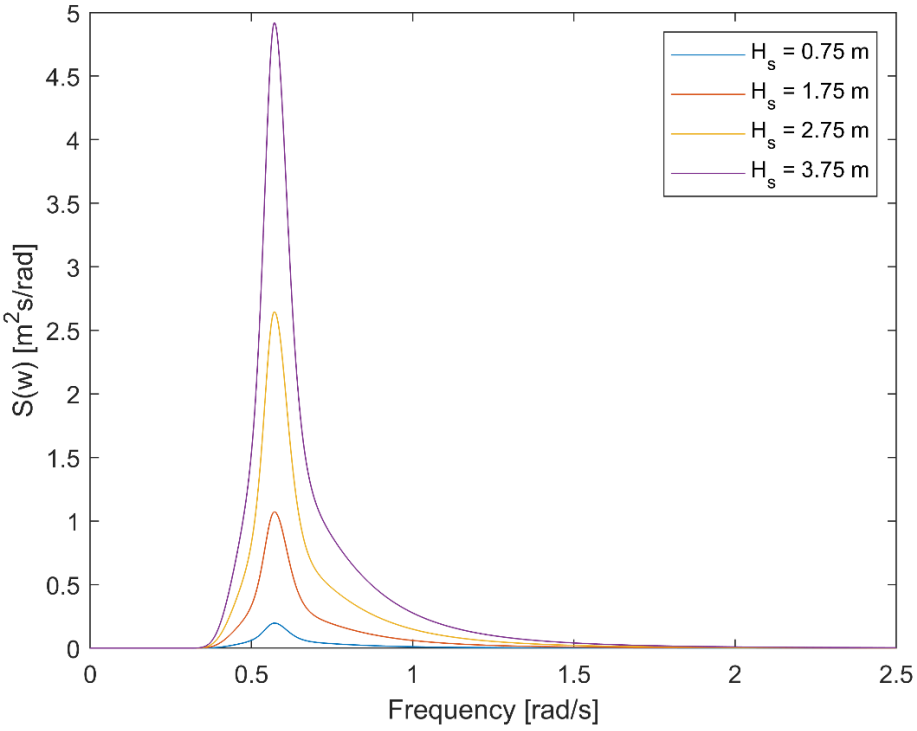

Figure 3. JONSWAP spectrum for $t_p = 11\ s$ with $H_s = 0.75\ m$, $H_s = 1.75\ m$, $H_s = 2.75\ m$, and $H_s = 3.75\ m$. S(w) represents the wave spectrum of the angular frequency, ω [rad/s].

Furthermore, the energy transport [kW/m] is defined as the transport of energy per unit width. For a real sea wave propagating in one direction the energy transport is described as [3]

$$J = \rho g \int_0^\infty c_g(f) S(f) df = \rho g^2 t_p H_s^2 / 64\pi \qquad (2)$$

where $c_g(f)$ is the group velocity and defined as $c_g(f) = g/4\pi f$ [m/s]. However, the distribution of energy varies both in time and space.

Sea states differ globally, leading to the capability to extract energy from the oceans' waves is geographically uneven as the energy content depends on the location. The most energetic waves exist in the latitude interval [± 40 º, ± 60 º] [1], see Figure 4. In addition to the geographical fluctuations, waves in one location vary on time scales ranging from a couple of seconds to years [3]. Wave periods are measured in 10^1 s, duration and intervals between wave groups are in the magnitude of 10^2 s, further, waves vary hourly, daily, monthly, seasonally, and yearly as well. The wave energy can be significantly higher in the winter months compared to the summer months, the average wave energy can for a winter month be 5-10 times higher than a summer month's average [3]. As a result of these large variations, there is a factor of two between the highest and the lowest annual mean for wave energy at one location [3]. WECs must be designed to operate under these various sea states conditions, both to be

optimized to harness the largest amount of energy during appropriate sea states but also to survive extreme weather.

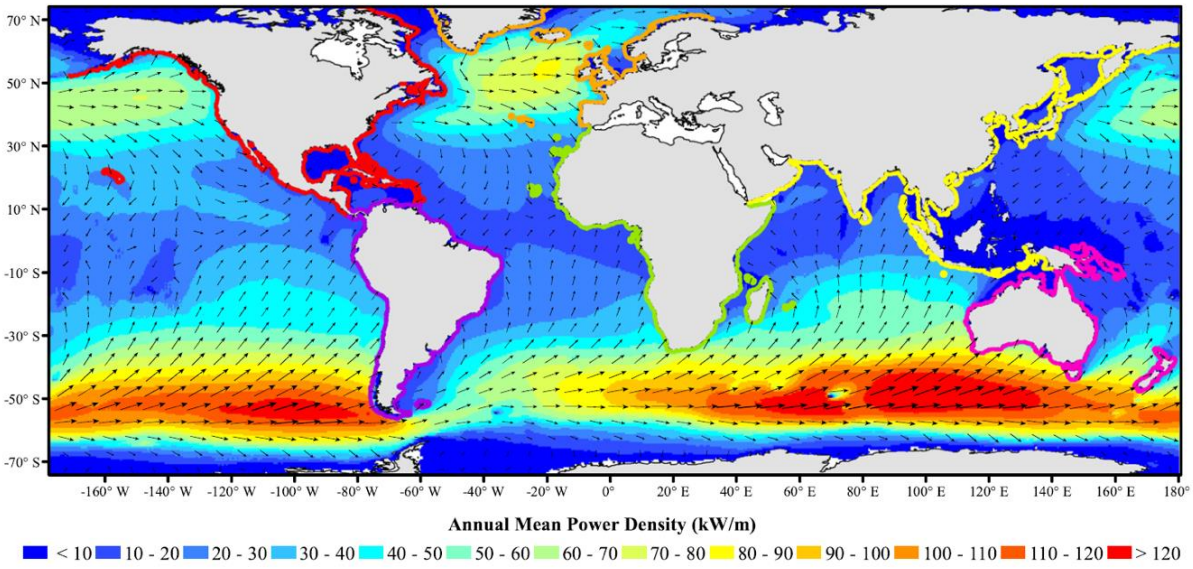

Figure 4. Global distribution of the annual mean energy transport (color) and the predominantly direction of it (arrow). Source: [1].

2.3 Wave energy converter devices

There are several technologies of harvesting wave energy utilizing the propagating motion of waves. The conceptual and operational principles of wave power technologies are diverse, as well is the location of the devices, indicating yet an immature technology [4]. A WEC is coupled to a power take-off (PTO) system where the device's absorbed energy is converted to electricity. WECs are usually characterized by location and type, within these two classifications the devices can further be categorized by their mode of operation. The following section aims to broadly map the different technologies as well as the wave power market by presenting some companies and their technologies to give this thesis a context of the wave power industry. The presented WEC devices are illustrated in Figure 5.

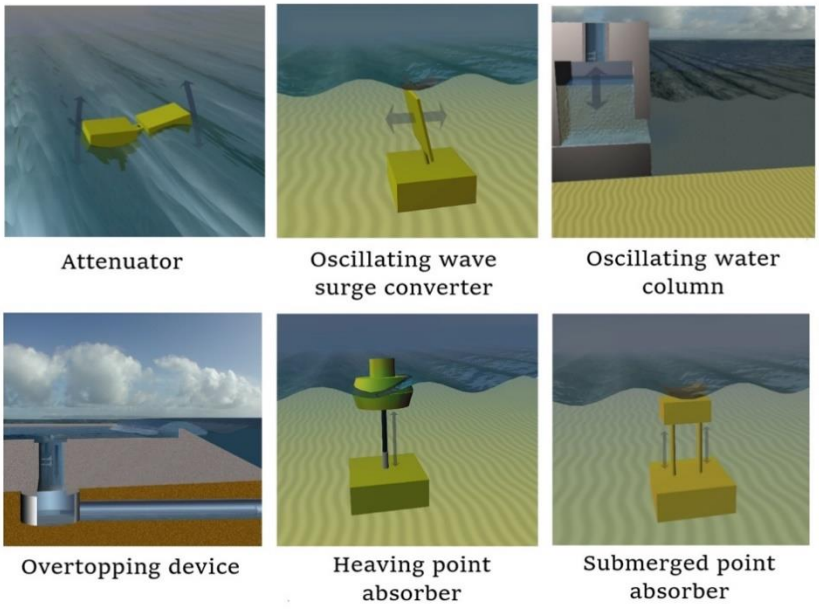

Figure 5. Different technologies of WECs. Picture source: [21]

2.3.1 Location

Energy harvesters are either located at shoreline, near shoreline or offshore [15]. The WEC devices located close to the shoreline have the advantages of a calmer wave climate reducing the damages caused by extreme sea states, their proximity to the electricity grids and that they are easier to maintain compared to devices located further away from the shoreline. However, the energy content is maximized in deeper water waves, thus, locating WECs in deeper waves enables the system to harvest the greatest amount of energy. Despite the technological challenges and the resulting increased costs offshore devices experience, it is argued that these technologies will be the most competitive in the market [15].

2.3.2 Type

As mentioned earlier, the conceptual principles of WECs are diverse with many variations in design, nevertheless, the concepts are often categorized by three dominant types: the attenuator, the terminator, and the point absorber. Compared to the point absorber, both the attenuator and the terminator are horizontally long relative to the wavelength, hence, they are being referred to as line absorbers.

The Attenuator

An attenuator lies parallel to the propagation of the wave, and thus the device rides the wave [15]. Pelamis was a Scottish based company producing a floating attenuator WEC. The shape and the motion of the Pelamis WEC was similar to a swimming snake with semi-submerged cylindrical structures linked by hinged joints [22]. These cylindrical structures moved relative to each other as the device rode the wave. The

concept behind Pelamis was to restrain the motion of the hinged joints by letting hydraulic rams serve as a PTO system by pumping fluid into high-pressured accumulators. Hydraulic motors were then used to pump a regulated flow from the accumulators to induction generators producing electricity. By letting the accumulator act as energy storage, the electricity generation was consistent. Lastly, the power generated in the Pelamis was transmitted to the shore via sea-cables. In 2014, Pelamis failed to secure enough funding to further develop their technology and as no buyer was found the company collapsed [23].

The Terminator

A terminator device is similar the attenuator in the sense that they both are designed as line-devices but opposed to the attenuator, the terminator lies perpendicular to the primary direction of propagation of the wave [15]. Following are some examples of terminators using different modes of operations.

Aquamarine Power developed the Oyster WEC that was an *oscillating wave surge converter*. The concept behind the nearshore-placed Oyster is explained in [24] and the authors described that the Oyster utilized the dominant surge forces which occur in nearshore locations with a water depth of 10-15 m. An oscillating wave surge converter consists of an oscillating bottom-hinged buoyant or flap with the shape of a column that fully penetrates the water from the surface to the seabed. The column is connected to the shore through a closed pipeline system with water as transport medium. As a result of the completely penetrating column, the oscillating buoyant is experiencing a wave force in the surge direction. This surging force drove hydraulic pistons that pressurized water and pumped it to the shore through the pipeline system. The pumped and pressurized water drove a hydroelectric plant on shore converting the energy to electricity. Lastly, the water was transported back to the column through the pipeline system. Aquamarine Power ceased trading in 2015 when the company did not find a buyer [25].

Wave Dragon is originally a Danish company that today are based in South Wales developing an *overtopping device* [26]. The principle behind an overtopping WEC is to collect water in a reservoir placed above the mean sea surface level [27]. The water in the reservoir is later led back to the sea level via a PTO system consisting of several hydro turbines which are connected to permanent magnet generators generating electricity. The wave Dragon has a relatively large size with an occupying area of 260 x 150 m, 300 x 170 m and 390 x 220 m depending on which wave climate the WEC is installed in [28]. The smallest size corresponds to a WEC located in a wave climate with an annual average wave power of 24 kW/m, the middle size to 36 kW/m and the biggest size to 48 kW/m. The different sizes of Wave Dragons have, in these conditions, an installed capacity of 4 MW, 7 MW and 11 MW respectively and have an annual power production of 12 GWh/y, 20 GWh/y and 35 GWh/y [28].

Australian based Wave Swell is another company utilizing the terminator type of WECs, but their mode of operation is in the form of an *oscillating water column*. An

oscillating water column can either be land-based located at the shoreline or be floating and consists of a semi-submerged air chamber [4]. Wave Swell's WEC is land-based and the air chamber is mounted to the shore. The concept behind Wave Swell's WEC is to let the device be an artificial blowhole forcing air in a pressured chamber to pass through a turbine generating electricity [29]. The chamber is open below sea level where water can rise and fall pressuring the air to rise to the turbine. Wave Swell is currently developing their first project in Tasmania, Australia, of 200 kW [30]. This project is later intended to showcase the cost effectiveness for larger project of 1 MW [31].

The Point Absorber

A point absorber is characterized by being much smaller than the propagating wave's wavelength [8]. The device can either be floating on the surface heaving up and down or be submerged below the water surface operating on pressure differential [15]. The fundamental principle of a point absorber is to extract wave motions relative a fixed reference point [16]. In contrast to the attenuator and the terminator, the point absorber is not dependent on the angle of wave incidence [15].

A *heaving point absorber* buoy experiences relative motion between the buoy and the reference point, this relative motion is later transferred to electricity by the PTO system. The PTO system is often direct and linear. Depending on the design, a point absorber can consist of one or two bodies [16]. A one-body point absorber merely consists of the buoy while a two-body point absorber has a submerged body attached to it. The submerged body increases the WEC system's inertia shifting the system's frequency response facilitating a resonant behavior with the incident wave [5]. There are several companies that have used or are using the point absorber type of a WEC, one of these companies being CorPower Ocean. The design and concept behind CorPower Ocean's heaving point absorber will in 2.5 CorPower Ocean's point absorber be explained in detail. Some other companies deploying or having deployed the point absorber are Ocean Power Technologies, Seabased and Wavebob. Ocean Power Technologies is an American company focusing on point absorbers serving as uninterruptable power supply systems for marine applications located offshore [32]. Their PB3 PowerBuoy has a capacity of 8.4 kWh/day [33]. Seabased was originally a spin-off company to Uppsala University's research on wave power, however, today the company has its office in Norway and focuses on production to the grid [34-35]. Wavebob was an Irish company utilizing the point absorber technology that 2013 due to funding difficulties had to close [36].

In contrast to the heaving buoy point absorber WEC, the *submerged point absorber* buoy relies on the pressure differential that arises from passing waves. AWS Ocean Energy is a Scottish based company that utilizes this concept of pressure differential. The submerged point absorber moves when variations in sub-sea pressure occur, that motion is through a direct-drive generator transferred to electricity [37]. The AWS

Ocean Energy device is used in a system configuring several devices for a rating between 25 kW and 250 kW and is suitable for water depth over 25 m [37].

Today the point absorber is seen as a candidate to be the leading technology in high energetic wave climates [16]. In Europe, where most research is carried out on WECs in general, the R&D is highlighted on point absorbers [38]. The attenuator and the terminator have the advantage of being able to extract much energy of the incident wave due to the length of the device, however, point absorbers are modular and can be installed in arrays creating a "wave park", similar to a line absorber increasing their energy extraction capacity. Moreover, the point absorber has the advantage of taking incident waves from all directions.

2.4 Fundamental principles of wave energy extraction

The Norwegian wave energy researcher Falnes [3], [39], explains that, paradoxically, a good wave absorber device must also be a good wave-maker. If a body capable of oscillating in water experiences an excitation wave the body will oscillate, and consequently, create a radiated wave. This radiated wave is inevitable and shall be considered a necessity. The fundamental principle of extracting energy from waves is to remove the waves' energy and convert the energy to preferred form. Therefore, for the reason of energy harvesting, the radiated wave must oscillatory displace the continuing propagation of the incident wave and doing so with the correct phase, see Figure 6.

The superposition of the different waves in Figure 6 illustrates complete absorption of a wave's energy if small bodies oscillating in one-mode were to be placed evenly in an infinite line perpendicular to the wave's propagating direction with the bodies placed less than one wavelength apart. Nearly complete absorption for a one-mode heaving body can only be achieved if the body is sufficiently non-symmetric. A symmetric body radiating symmetric waves, as case b) in Figure 6, can theoretically absorb 50 % of the incident wave's energy while a symmetric body radiating non-symmetric waves, as case c) in Figure 6, can impossibly absorb more than 50 % [39].

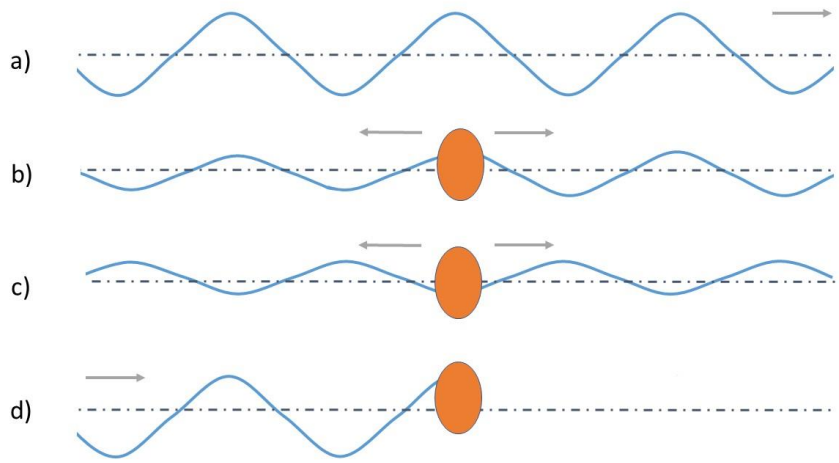

Figure 6. "To destroy a wave means to create a wave". Illustration a) represents an incident wave propagating in the direction of the arrow. Illustration b) demonstrates the symmetric radiated waves a symmetrical body heaving in one-mode can generate. Illustration c) demonstrates the antisymmetric radiated waves a symmetrical body heaving in one-mode can generate. Illustration d) represents complete absorption of the incident wave and is a superposition of the above curves. Figure based on [39]

2.4.1 Resonance and control methods

A WEC system oscillating in one-mode, i.e. in the heave direction, has an optimum phase condition when the system is in resonance with the incident wave [39]. If the WEC system is oscillating with a frequency equal or close to the system's natural frequency, resonance occurs and as mentioned, resonance amplifies the device's amplitude, as well as its speed. In resonance, the oscillatory velocity of the WEC system is in phase with the excitation wave providing maximum power output. When a system oscillates at the resonant frequency, the stored energy in the system is constant; the system is alternating between kinetic energy and potential energy of the same size [40]. As opposed to other naval structures, WECs tend to operate close to their natural frequencies to optimize the power output [41].

A WEC must have a large mass to be in natural resonance with the incident wave. Nevertheless, optimum phase conditions are approximately fulfilled for frequencies slightly off resonance as well [39]. Frequencies approximately satisfying optimal phase conditions constitute the system's so-called resonance bandwidth. Large enough WEC devices will have broad bandwidths, however, large WEC are costly and will not be competitive in the market. For that reason, smaller and more reasonable sizes of WEC devices with narrower bandwidth are used and control methods are applied to achieve a broader bandwidth and optimum motion instead [3]. There are various ways to control a WEC system, below three different control methods will be presented: latching, reactive control, and model-predictive control.

Latching control

Ringwood, Bacelli and Fusco [4] explains that latching can be thought of as a discrete control method since it is either "on" or "off". With latching control, the motion of the buoy is locked at various points in the wave cycle where the device velocity is zero and released when the buoy is in phase with the incoming wave, see Figure 7. Despite that the device velocity is zero for longer periods of the wave cycle, latching control optimizes the phase between the device motion and the excitation wave, and thus, the overall energy capture is maximized. Falnes and Hals [8] explains that latching control is a suboptimal method for the reason it achieves close to perfect phase alignments.

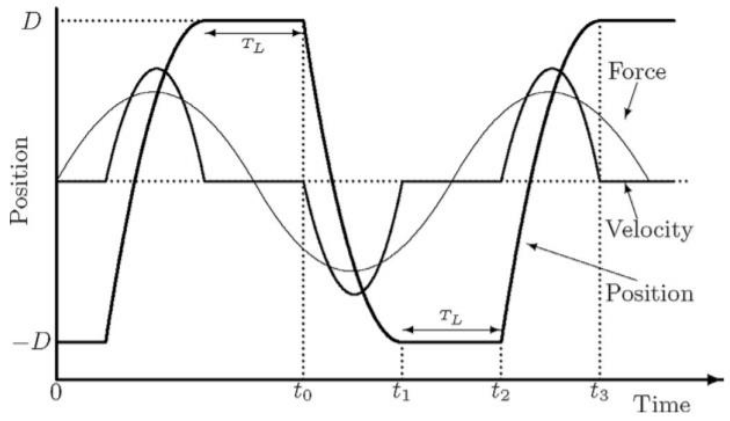

Figure 7. Latching control of a WEC. The force represents the force from the incident wave, the position and the velocity refer to the WEC's position and velocity, and T_L is the time the WEC is latched. Source: [42].

Reactive control

Reactive control, on the other hand, is an optimal continuous-time control method as it achieves perfect phase alignments. Maximum energy absorption occurs when the machinery impedance cancels the intrinsic impedance of the mechanical wave-body system [43]. Reactive control minimizes the reactance through reversed flows from the PTO system during parts of the oscillation cycle [8]. The reactive forces from the PTO system reduce the reactance of the wave-body system providing optimized energy capture since the device velocity and the excitation wave are in phase when there is no reactance. In comparison to the illustration of latching in Figure 7, the velocity would with reactive control align and be in phase with the excitation force, and the position would have a phase shift of $\pi/2$ in relation to the force and the velocity.

Model-predictive control

Hals, Falnes and Moan [43] states that constraints on motion amplitudes, machinery forces and possibly other features should be considered when implementing a control method for real WEC devices. A control method suitable for accounting constraints is the model-predictive control (MPC) strategy. The general approach of MPC is to define

an optimization problem where constraints and the optimization function are specified by the designer. When maximizing the energy output in a WEC device with constraints set on the machinery forces, a requirement is that the controller has sufficiently prediction of the wave excitation force. There are various ways to predict the excitation force. [44] explains that Autoregressive and Autoregressive Moving Average models, as well as Kalman filters can be utilized for the purpose of excitation force prediction, and [45] presents deterministic sea wave prediction as another method to predict the excitation force.

Figure 8 illustrates a comparison of the three abovementioned control methods done by [43]. The comparison is in relation to the Budal diagram, the theoretical upper bounds for power absorption which in the figure are represented with black dashed lines. The comparison of the three control methods below is not narrated for in detail, the interested one can see [43] for a more detailed description of the differences in the three methods. The optimal control refers to the control only constrained by the heave position of a heaving point absorber to $\pm 3\,m$ with an incident wave with wave height $1\,m$. Further, the black line represents the potential a MPC controller possess if the controller has precise prediction of future incident waves, the red dashed line a reactive controller restricted to sinusoidal motion, and the green dashed line a latching controller. Additionally, the figure also includes a scaled comparison between the optimal and the MPC controllers represented with the grey line with diamonds on, however, this will not be further regarded in this thesis. As outlined in Figure 8, MPC is the control method maximizing the power absorption, followed by the reactive control and latching.

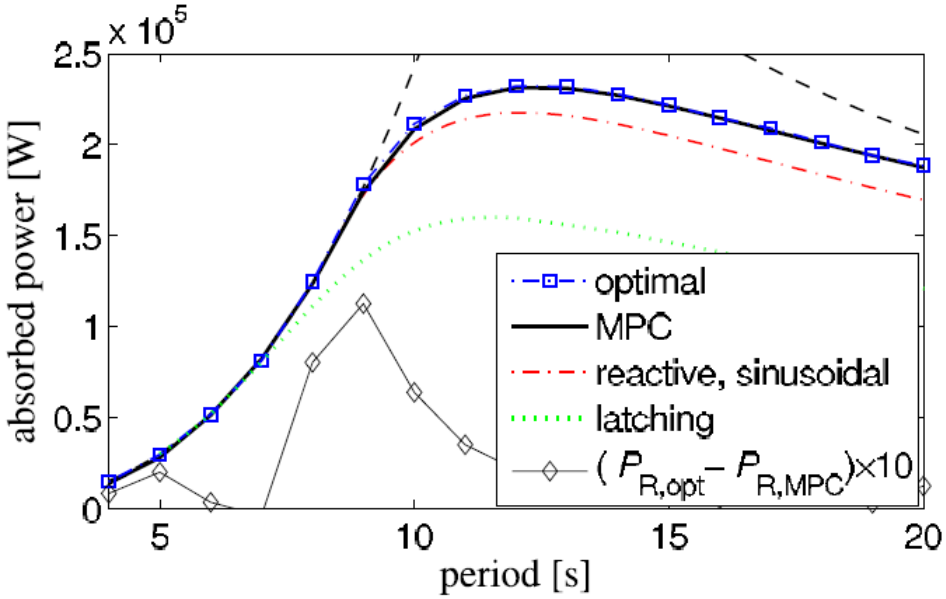

Figure 8. Comparison of the three control methods of MPC, reactive control, and latching in comparison to an optimal control and the theoretical upper bounds (black dashed line), also known as the Budal diagram. Source: [43].

CorPower Ocean utilizes a combination of control methods to increase the annual energy production. In regular operational waves a MPC approach is deployed while in more high energy operational waves MPC is used together with latching.

2.5 CorPower Ocean's point absorber

CorPower Ocean's WEC consists of a floating buoy anchored to the sea bottom by mooring wires, see Figure 9. The WEC has one oscillating part and one stationary part providing the relative linear motion that is later converted to electrical energy. The oscillating part is made up of the buoy consisting of a hull and components mounted to the hull. For instance, a rack is mounted to the hull which constitutes the relative motion and drives the machinery in the PTO system. The buoy moves vertically up and down in relation to a slide that is attached to the sea bottom through the mooring system. The slide constitutes the stationary part and is vertically positioned through the pretension cylinder which is described in more detail below. The buoy and the slide are always in alignment with the tensioned mooring wires and the anchor point, but the system can move freely around the anchor point.

Two gearboxes and two generators are mounted to the slide converting electricity from the heaving rack. There is a tide regulating system on the mooring lines adjusting the buoy's position in relation to the surface level variations caused by tide. The buoy will in full scale be 9 m in diameter and weigh close to 28,000 kg and the installed capacity will be 0.5 MW per WEC. The WECs will be installed in arrays at water depths around 45 m and be connected to the grid via sea cables on the sea bottom. Following will some key components of CorPower Ocean's WEC be specified in more detail.

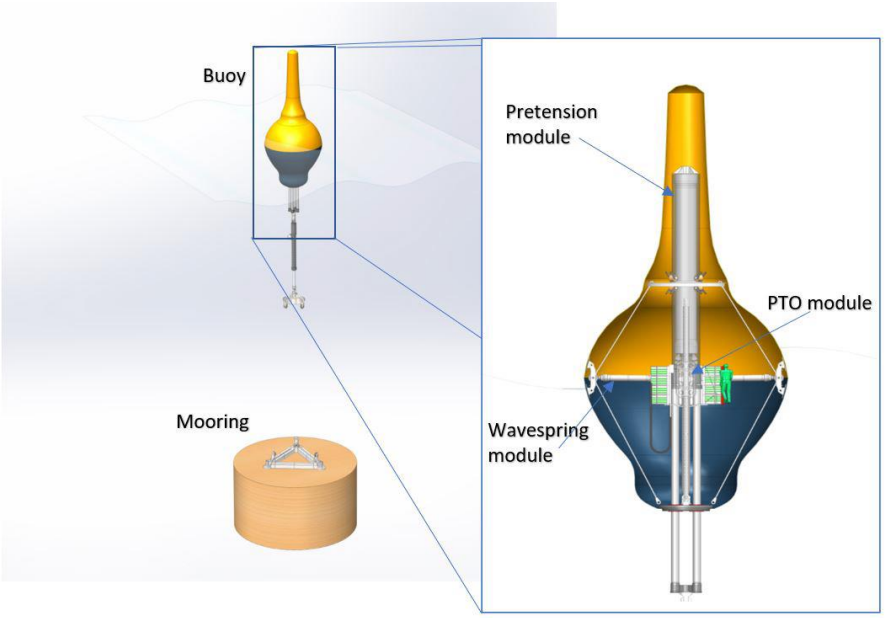

Figure 9. Illustration of CorPower Ocean's WEC. Figure provided by CorPower Ocean.

2.5.1 Pretension cylinder

In order to balance a buoy at its midpoint, the buoy must have a large mass. CorPower Ocean's WEC, on the other hand, is lightweight due to a pretension cylinder creating a downward force on the buoy replacing the otherwise required additional mass. The light weight gives the WEC the characteristics of having a low natural frequency in heave, lower than all wave periods in the ocean providing the WEC high survivability in storms. The pretension cylinder is stationary mounted aligned with the mooring wires and do not oscillate with the buoy.

2.5.2 WaveSprings

CorPower Ocean's WEC is equipped with two WaveSprings acting as negative springs counteracting the hydrostatic heave force. The hydrostatic force will be specified in section 2.6.2 Forces acting on the buoy. A WaveSpring consists of a pneumatic cylinder with a pressurized main chamber and has a vertically constant axial force. The WaveSprings are semi-oscillating and semi-stationary as they are mounted both to the oscillating hull and the stationary slide. The WaveSpring mechanism provides additional phase control and allows the WEC to be in resonance with the wave climate and amplifies the motion over a wide bandwidth in operational mode. The WaveSprings amplifies the heave motion by a factor of three compared to the incident wave. However, the WaveSpring mechanism is deactivated in rough sea states, making the lightweight WEC transparent to extreme waves increasing the survivability.

2.5.3 PTO module

In the PTO system, two gearboxes convert the linear motion to rotational motion in an efficient way. The rotational motion is later converted to electricity through direct driven generators. There are two generators, one that is engaged when the buoy moves up and the other one is engaged when the buoy moves down. The generated electricity in the PTO module is delivered to the grid.

2.6 Theory

The following section is aimed to give the reader the necessary theoretical background to further understand the investigation. Both the coordinate systems the WEC are referenced in and the hydrodynamic forces that act on the buoy are presented. CorPower Ocean has developed a model of the WEC in the time domain. For that reason, the acting forces on the WEC system will also be regarded in the time domain.

2.6.1 Coordinate system

The position of a buoy is defined by a coordinate system of six degrees of freedom, see Figure 10. The buoy can move in the translational directions x, y, z as well as rotate around the x, y, z axes. The naming convention of the positions in relation to the axes is

generally surge, sway, heave, for the translational positions, $[x, y, z]$, and roll, pitch, yaw for the rotational positions around the translational axes, $[\phi, \theta, \psi]$.

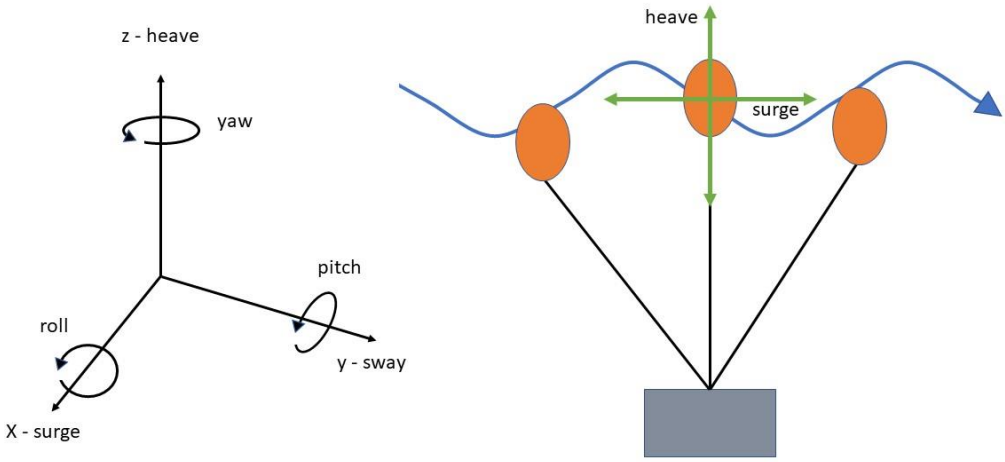

Figure 10. Coordinate system of a WEC. The wave is propagating in the surge direction.

Global reference frame and body reference frame

In order to calculate the precise position of the buoy, a global reference frame and a body reference frame are needed. The global reference frame's origin is located on the mean surface level with the heave axis pointing vertically upwards. Figure 11 demonstrates the global and the local reference frame. The transformation between the global and the body reference frame is mathematically done with transformation matrixes using Tait-Bryan angles. The local coordinates $\boldsymbol{r}^B$, can be transformed to global coordinates, $\boldsymbol{r}^G$, with the transformation matrix $\boldsymbol{R}$, $\boldsymbol{r}^G = \boldsymbol{R}\boldsymbol{r}^B$, or vice versa, the global coordinates can be transformed to local coordinates with $\boldsymbol{r}^B = \boldsymbol{R}^T\boldsymbol{r}^B$, where $\boldsymbol{R} = \boldsymbol{BCD}$,

$$\boldsymbol{B} = \begin{bmatrix} 1 & 0 & 0 \\ 0 & \cos(\phi) & \sin(\phi) \\ 0 & \sin(\phi) & \cos(\phi) \end{bmatrix}, \boldsymbol{C} = \begin{bmatrix} \cos(\theta) & 0 & -\sin(\theta) \\ 0 & 1 & 0 \\ \sin(\theta) & 0 & \cos(\theta) \end{bmatrix}, \boldsymbol{D} = \begin{bmatrix} \cos(\psi) & \sin(\psi) & 0 \\ -\sin(\psi) & \cos(\psi) & 0 \\ 0 & 0 & 1 \end{bmatrix}$$

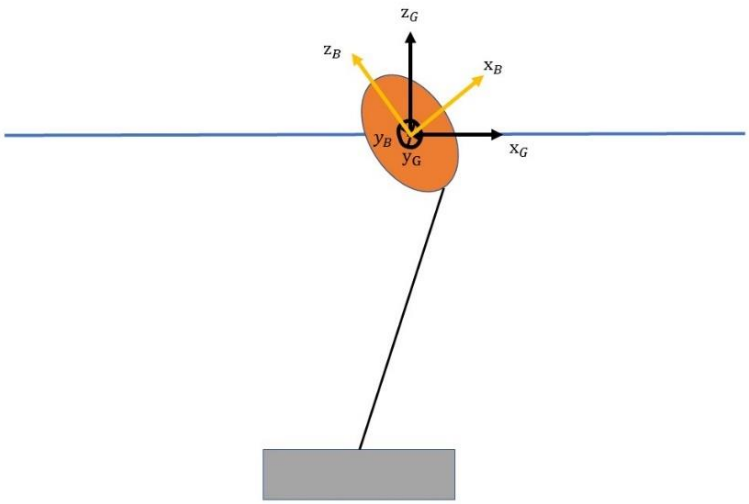

Figure 11. Global and body reference frame.

2.6.2 Forces acting on the buoy

The forces the WEC experiences from the waves are referred to as hydrodynamic forces. In addition to the hydrodynamic forces, the WEC experiences forces from the buoy's inside coupled to the PTO system which are referred to as machinery force.

Four different hydrodynamic forces are considered in CorPower Ocean's model: the buoyancy force, the radiation force, the excitation force, and the drag force. Following below will these forces on the buoy be described.

Further, CorPower Ocean's model considers four machinery forces: a transmission force from the energy conversion device, a pretension gas spring force, a WaveSpring gas force, and a friction force from the PTO system. However, the machinery forces will in this thesis be regarded as the resulting force referred to as $\boldsymbol{\tau}_{PTO}$.

Buoyancy force and hydrostatic force

The buoyancy force is the upward force exerted by the fluid on a submerged body which enables the body to float if the sum of the buoyancy force and the gravity force is positive [41]. In CorPower Ocean's model the buoyancy force is regarded as one of the hydrodynamic forces.

The resulting force composed of the buoyancy force together with the gravity force is called the hydrostatic force. The hydrostatic force is constantly striving to reach the equilibrium of the buoy; therefore, it is often referred to as a restoring force. Both the buoyancy force and the gravity force are active in the heave direction, however, when the buoy is displaced from its equilibrium position (global reference frame), the hydrostatic force can be active in all components (body reference frame) restoring the

buoy to its equilibrium. The buoyancy force is, in the global reference frame, calculated as

$$\boldsymbol{\tau}_{buoyancy}(t) = \rho g V_{sub}(t)\overrightarrow{\boldsymbol{e}_z} \quad (3)$$

where ρ is the density of water, g the gravitational acceleration, $V_{sub}(t)$ is the instantaneous submerged volume of the buoy and $\overrightarrow{e_z}$ is the unit vector in heave. Furthermore, the gravity force is, in the global reference frame, calculated as

$$\boldsymbol{\tau}_{gravity} = -m_b g\overrightarrow{\boldsymbol{e}_z} \quad (4)$$

where m_b is the buoy's mass. As mentioned, CorPower Ocean's buoy is lightweight and in order to keep the buoy at equilibrium a pretension force is established to pull the buoy down. The pretension force is, in the global reference frame, active in the heave direction and is calculated as

$$\boldsymbol{\tau}_{pre} = p_{0,pre}A_{piston} \quad (5)$$

where $p_{0,pre}$ is the initial pressure in the pretension cylinder and A_{piston} is the cylinder's net active area. In equilibrium, the balance of the hydrostatic force and the pretension force is

$$\boldsymbol{\tau}_{pre} + \boldsymbol{\tau}_{buoyancy} + \boldsymbol{\tau}_{gravity} = 0 \quad (6)$$

Radiation force

A body experiences a radiation force when the body is moved in an otherwise calm water [41]. The radiation force is due to the motion of the structure and the radiated wave an oscillating body creates [46]. In the time domain the radiation force can be calculated as [46]

$$\boldsymbol{\tau}_{rad,tot} = -\boldsymbol{m}_\infty\ddot{\boldsymbol{x}} - \int_0^t \boldsymbol{K}(t-t')\dot{\boldsymbol{x}}(t')dt' \quad (7)$$

where $\boldsymbol{m}_\infty$ is the constant positive definite added mass matrix, $\boldsymbol{x}$ is the position vector of the buoy, hence, $\dot{\boldsymbol{x}}$ is the velocity vector and $\ddot{\boldsymbol{x}}$ the acceleration vector, the convolution $\boldsymbol{K}(t)$ is the matrix of retardation or memory functions. The radiation force is commonly referred to be composed of the added mass force proportional to the body acceleration (first term) and the damping force proportional to the body velocity (second term) [41]. The added mass is due to the additional mass of water a moving body experiences.

Excitation force

The excitation force is the force a body experiences when the body is kept fixed in the incoming waves and is a pressure force induced by the incident wave [40]. The result of the induced pressure from the incoming wave is a velocity potential on the wetted

surface of the body. A velocity potential is the scalar describing the magnitude of the fluid's velocity if the fluid is assumed to be incompressible, irrotational, and non-viscous [40]. The velocity potential is constituted of two parts, one from the undisturbed incident wave and the other from the resultant diffracted wave. A diffracted wave will occur when the undisturbed incident wave does not satisfy the homogenous boundary condition on the fixed wet surface (see [40]). The excitation force is calculated as [16]

$$\boldsymbol{\tau}_{exc} = \iint_{wetted\ surface}^{body} \boldsymbol{p}_{wave}\, \boldsymbol{n} dS \tag{8}$$

where $\boldsymbol{p}_{wave}$ is the pressure of both the incident wave potential and the diffracted wave potential, n the normal vector and S the wetted surface. Hence, the integration is over the body's wet surface, in other words the submerged surface. As the velocity potential is dependent on the incoming wave, the excitation force is also dependent on the incoming wave.

Drag force

The drag force is due to water friction and is mainly caused by vortex shedding occurring when water flows past the WEC's body [41]. The relation between the drag force and the relative velocity between the buoy and the water is quadratic. The drag force can for the translational modes be expressed as

$$\tau_{drag,i} = \frac{1}{2}\,\rho A_{sub,i} C_{D,i} u_{rel}(v_i - U_i), \qquad i \in [1,2,3] \tag{9}$$

where ρ is the density of water, $A_{sub,i}$ the projected area in direction i perpendicular to the direction of motion, $C_{D,i}$ is the drag coefficient in direction i, v_i and U_i are the velocities of the body and the water in direction i. The relative velocity between the buoy and the water, u_{rel}, is calculated as

$$u_{rel} = \sqrt{\sum_{j=1}^{3}\left(v_j - U_j\right)^2} \tag{10}$$

For the rotational modes, the drag force is only dependent on the body motion, therefore it can be expressed as

$$\tau_{drag,i} = \frac{1}{2}\rho A_{sub,i} C_{D,i} |v_i| v_i \qquad i \in [4,5,6] \tag{11}$$

To summarize the hydrodynamic forces, all the forces are in some way affected by the characteristics of the incoming wave. However, the force from the wave is, solely, represented by the excitation force. Moreover, the radiation force, the hydrostatic force, and the drag force are effects of the buoy's response from the excitation such from the resulting buoy motion and submergence level. The hydrodynamic forces are generally large, the magnitude of the forces in surge are often represented in the range 10^5-10^6 N. Figure 12 shows time series demonstrating the ratio between the hydrodynamic forces

in surge in the body reference frame for an operational scenario of CorPower Ocean's WEC.

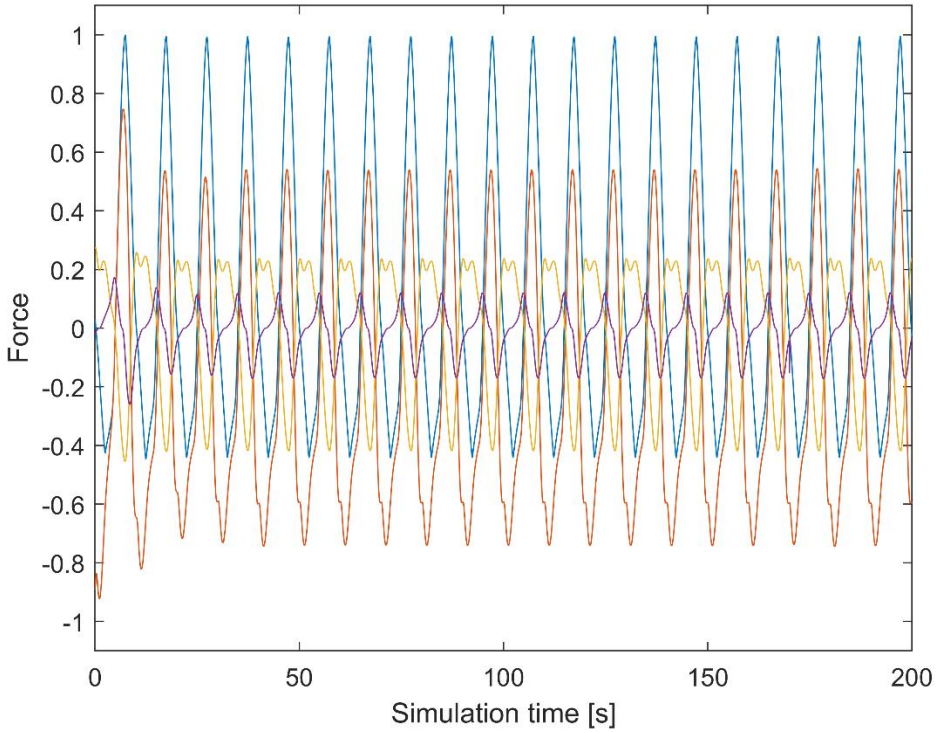

Figure 12. Normalized hydrodynamic forces in surge for a typical operational scenario with an incident wave with H_s = 4m and t_p = 10s in the body reference frame.

Dynamic equation of the system

The motion of the buoy relies on Newton's second law of motion and can be expressed as a differential equation with the hydrodynamic forces illustrated above together with the mechanical forces in the PTO system

$$\left(\boldsymbol{I}\left(m_{buoy} + m_{PTO}\right) + \boldsymbol{m}_{\infty}\right)\ddot{\boldsymbol{x}}_{buoy} = \boldsymbol{\tau}_{exc} + \boldsymbol{\tau}_{hyst} + \boldsymbol{\tau}_{rad} + \boldsymbol{\tau}_{drag} + \boldsymbol{\tau}_{PTO} \quad (13)$$

where $\boldsymbol{I}$ is the identity matrix, m_{buoy} and m_{PTO} the mass of the buoy and the PTO system respectively, $\boldsymbol{m}_{\infty}$ is the added mass matrix coupled to the radiation force, and $\ddot{\boldsymbol{x}}_{buoy}$ is the acceleration of the buoy in the direction of the wire system. $\boldsymbol{\tau}_{hyst}$ is the resulting hydrostatic force composed of the buoyancy force, the gravity force, and the pretension force.

2.7 CorPower Ocean's model

CorPower Ocean has developed a model of the WEC system in the MATLAB based graphical simulation interface Simulink. The model reflects the full coordinate system and has six degrees of freedom; thus, it can describe the exact position of the buoy. Moreover, the principle of the model is based on the dynamic equation of the system,

equation (13). It should be noted that the model is theoretically more elaborate in detail, nonetheless, the presented theory gives an accurate overview of the system for this thesis' purpose. The model has continuously been validated on data from physical tests in tanks and the ocean and the model has been refined to represent the actual WEC system in a sufficiently accurate way. Furthermore, the model is of conservative character, meaning the model represents an extreme scenario of known parameters. The mooring tension is amplified by 20 % compared to the measured physical value in tank tests. The load is amplified in the model to be sure the model is not an underestimation of the reality. In the WEC industry it is standard to use a conservative model.

In small waves which result in small device motions, the effects on the WEC can be approximately assumed to be linear [4]. However, in more realistic operational modes with larger waves and larger device motions, the effects on the WEC become predominant nonlinear [4]. The effects of the nonlinearity are further increased in WECs as they typically amplify the motion to maximize the power capture [4]. CorPower Ocean's model accounts for these nonlinearities.

An accurate model is an important tool in the development of WECs. Ringwood, Bacelli and Fusco [4, p. 35] states that the purposes of having a mathematical model of the WEC system are multiple, models are utilized for the purposes of:

- assessment of power production
- assessment of loading forces under extreme sea conditions
- simulation of device motion, including evaluating the effectiveness of control strategies
- for use as a basis for model-based control design

A model enables the developers to simulate the envisaged system and see if the response of the device is as desired. If not, the system can be further developed or controlled without high costs.

CorPower Ocean's model consists of a main model which constitutes smaller model blocks that mathematically describe different parts of the WEC. There are four sub-models: the hydrodynamic block, the controller block, the mooring system block, and the PTO block. An overview of the model can be seen in Figure 13. The main model merges the different blocks into one system of partial differential equations.

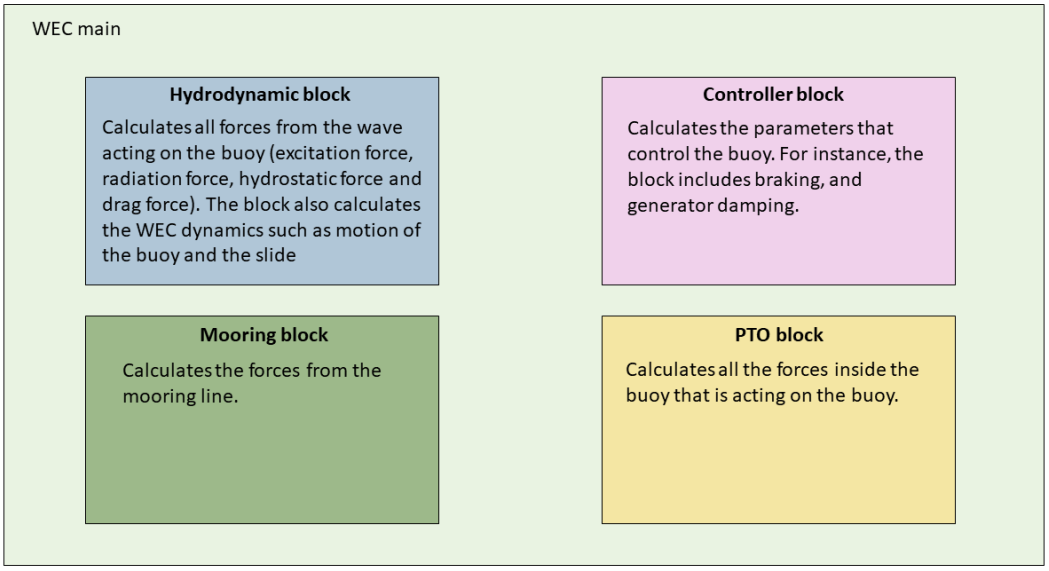

Figure 13. Overview of the WEC model.

3. Methodology

The methodology section describes and motivates the methods that have been developed and utilized to fulfill the purpose of the thesis. Firstly, the investigation's point of departure is explained, thereafter, the delimitations associated with the work. Lastly, two different methods, forced oscillation and linearization, are presented.

3.1 Point of departure

The device resonance response was examined through numerical simulations and the investigation had CorPower Ocean's model of the WEC system as its point of departure. It is worth noting that a model is a simplified representation of a real system, however, since the model is well tested the results were assumed to have a high credibility compared to the real WEC structure. A WEC is a coupled system, the different parts of the system influence each other. For instance, the hydrodynamic forces affect the machinery in the PTO system, and the PTO system affects the hydrodynamic forces. The investigation was centered around was the hydrodynamic block since it is a good indicator how the buoy's motion is affected by the incident waves.

Furthermore, the research questions regard when and how resonance in the surge mode occurs, therefore, the study investigated how the WEC system was affected by incoming waves of different frequencies. As resonance is coupled to oscillations of a specific frequency, the principal approach of the investigation was to find a frequency response of the buoy through simulations. Every simulation had a running time of 200 s. This simulation time was long enough to see eventual trends associated between the

WEC system and the corresponding wave period. Although the prominently wave periods at the sites CorPower Ocean is planning to deploy their WEC is in the interval $t_p = 8 - 11.5\ s$, and wave periods greater than that interval is unlikely, this thesis work regarded wave periods up to $t = 30\ s$. The purpose of regarding such long waves was to enable investigation of whether there were any trends associated with the surge resonance.

3.2 Delimitations

The purpose of this thesis was to investigate resonance in surge; therefore, the work was centered around motion and forces along the surge direction. Nevertheless, the investigation did also consider the heave component. The performance of the WEC is strongly coupled to heave motion as the PTO system utilizes relative motion in heave, for the reason of performance, the heave component was also included. No other directions were considered in the work.

The device resonance response was restricted to the response from the buoy, no other parts of the WEC system were considered. The investigation was limited to regular waves, all waves were unidirectional, and the wave front had a perpendicular incidence to the WEC.

3.3 Forced oscillation

The frequency response of a WEC system can be found by forcing the system to oscillate with regards to aspects of interest, i.e., for this thesis' purpose, letting the buoy have an excitation force only in surge. By "decoupling" the system and restricting the buoy to have a dominant excitation motion in surge, the dynamics related to the surge excitation will be highlighted.

As mentioned in the theory section, the excitation force is the force most strongly coupled to the incident wave and influences the motion of the buoy the most. For that reason, the excitation force was replaced with a sine wave in one direction while the other components were set to zero. Thus, the buoy was forced to only be hit by the incident wave in that one direction, for instance, the buoy was solely hit by the surge component of the incident wave. This forced excitation enabled investigation of how the buoy's motion was affected by that specific component of the excitation. The WEC was forced to have an excitation in surge and heave, separately.

The buoy's heave motion was assumed to have the same frequency as the incident wave. Nevertheless, the surge excitation frequency is not necessarily equal to the frequency of the incident wave. To clarify these two different frequencies, the buoy's surge period is referred to as *oscillation period* and the buoy's heave period is referred to as *wave period*. The purpose of letting the buoy oscillate with a forced motion in both surge and heave was to find the buoy's resonance frequency in surge as well as to

investigate how the surge motion responds to various frequencies of the incident wave. Forcing the buoy to only be excited in surge enabled investigation of which oscillation periods the surge motion was amplified. Further, forcing the buoy to only be excited in heave allowed observation of how the surge resonance is coupled to the frequency of the incident wave.

The height of the incident wave was set small (h_s = 0.001 m) to initially minimize the other hydrodynamic forces, with the result of letting the excitation force be the dominant force on the buoy. The forced excitation sinusoidal was defined with an amplitude representing the magnitude of the force. Different amplitudes on the excitation force were simulated to see how the magnitude of excitation affected the motion. For the surge case, the amplitude of excitation was set to 1,000 N, 20,000 N and 40,000 N, respectively. In a real scenario, compared to the forced oscillation case, the buoy will be less affected by such an amplitude since the forced oscillation is a restricted scenario dominated by the excitation force. For forced oscillation in heave, the amplitude of the excitation force was set to 50,000 N, 150,000 N and 250,000 N. The magnitude of the buoyancy force is constantly large in the heave direction with a magnitude close to 1,000,000 N, consequently, the excitation amplitude had to be large to simulate a reasonable scenario where the excitation force had an impact on the buoy. The "forced oscillation" approach for surge is illustrated in Figure 14.

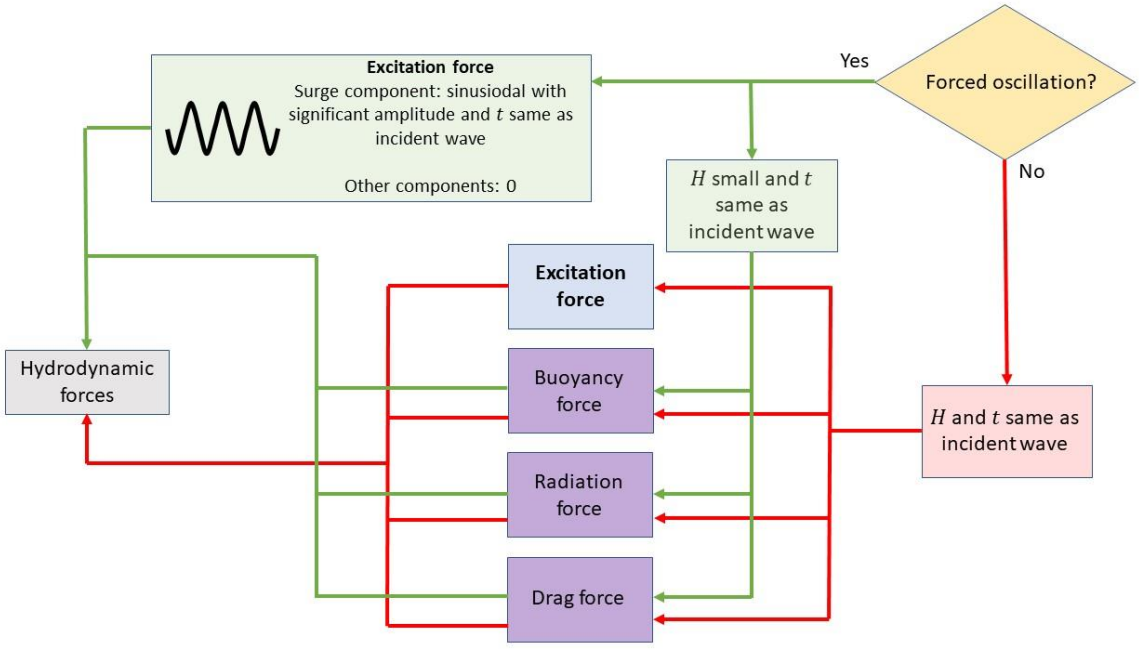

Figure 14. Illustration of the forced oscillation method. This illustration is representing forced oscillation in surge. Similarly, for forced oscillation in heave the heave component of the excitation force was replaced by a sinusoidal and the remaining components set to 0. The hydrodynamic force is later an input in the buoy block which calculates the position and the velocity of the buoy as illustrated in Figure 15.

3.4 Linearization

A nonlinear system can be approximately linearized in a small region around an operating point. The approximation is good near the operating point and is based on a first order Taylor expansion. A linear system is governed by the superposition principle and such a system can, unambiguously, be determined by its frequency response $G(i\omega)$ [47]. Ljung and Glad explains that [47] one of the advantages with determining a system by its frequency response is that it is easy to investigate interesting regions of frequencies, such as resonance frequencies.

Further, Ljung and Glad explains that the operating point is generally a steady state such that, if the system is modelled by the state space model

$$\dot{x} = f(x,u) = Ax + Bu \quad (14)$$
$$y = h(x,u) = Cx + Du \quad (15)$$

where u is the input, y the output and x the states, the steady state fulfils $f(x,u) = 0$. Nevertheless, a system does not necessarily need to be linearized around a steady state, it can be linearized at any state. However, if linearized at an arbitrary state, the linearized system is generally time variant. Moreover, it is often difficult to quantitively estimate how good the linearization of the system is. For that reason, conclusions based on the linearization should be carefully treated, and if possible, the approximation should be compared with an accurate nonlinear simulation of the system.

For a nonlinear Simulink model, the toolbox "Simulink Control Design" can be utilized for linearization of a system. The toolbox enables linearization of specific parts/components of the model. Simulation can be used to generate operating points through simulation snapshots. In that case, the operating point contains input levels and state values of the model at the corresponding snapshot time [48]. The result of the linearization is a linear state space model, a transfer function, and a zero-pole gain model, these representations can then be used to produce, i.e., bode plots [48].

Figure 15 is illustrating the system that was linearized in this thesis work. The position of the buoy is calculated in the "Buoy block" having the inputs "hydrodynamic force" and "other forces". The forces from the PTO system and the gravity force are two of the forces constituting the "other forces", however, the sum of these forces is small compared the hydrodynamic force, see Figure 16.

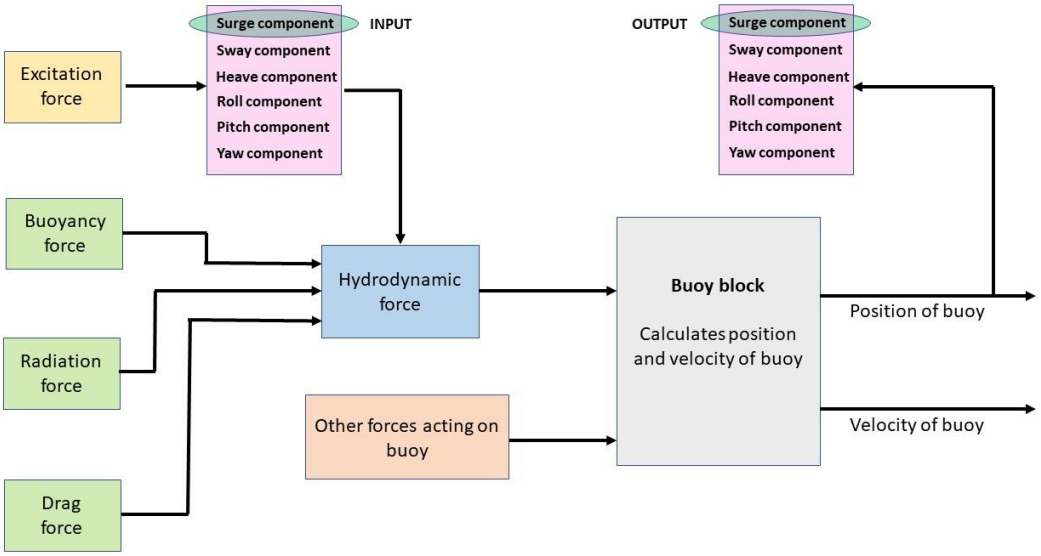

Figure 15. Illustration of linearized systems. The input of the system is the surge component of the excitation force. The output of the system is the surge component of the position of the buoy. The "other forces" block represents the non-hydrodynamic forces affecting the position and velocity of the buoy.

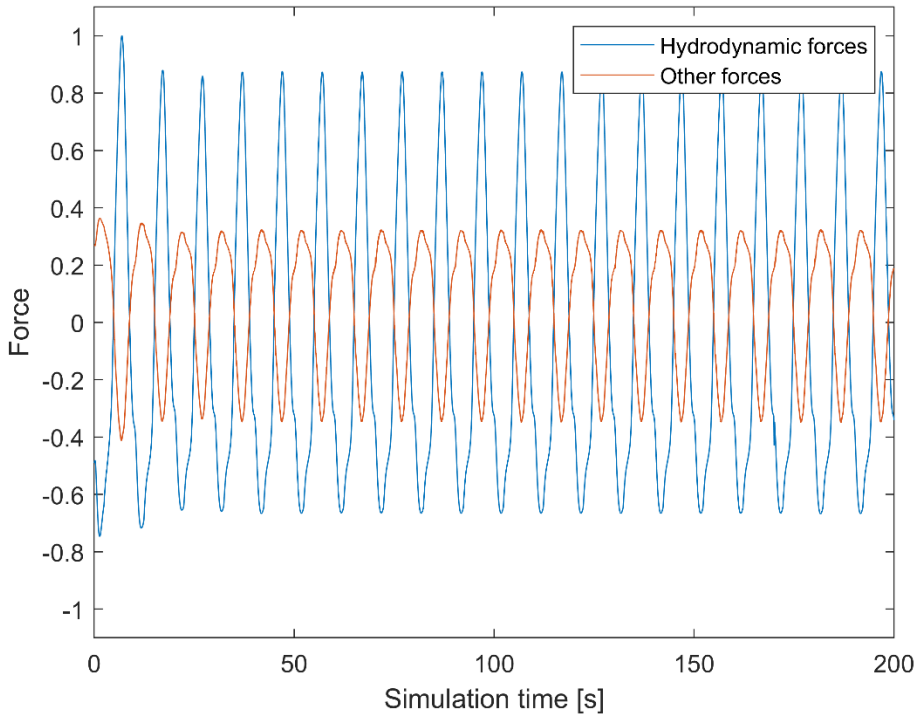

Figure 16. Plot illustrating the normalized ratio of the magnitudes between the hydrodynamic forces and the other forces in surge. The figure represents an operational scenario with an incident wave characterized by $t = 10\ s$ and $H = 4\ m$ and is presented in the body reference frame.

3.4.1 Eigenvalue and eigenvector analysis

Eigenvectors and eigenvalues are defined as [49, p. 295]

> If A is an $n \times n$ matrix, then a nonzero vector $\boldsymbol{x}$ in R^n is called an eigenvector of A if $A\boldsymbol{x}$ is a scalar multiple of $\boldsymbol{x}$, that is
>
> $$A\boldsymbol{x} = \lambda\boldsymbol{x}$$
>
> for some scalar λ. The scalar λ is called an eigenvalue of A, and $\boldsymbol{x}$ is said to be an eigenvector corresponding to λ.

When eigenvectors and eigenvalues are applied on structural systems, they contain information about the natural frequencies and the mode shapes corresponding to those frequencies. A natural frequency is, solely, dependent on the structure of the system [50]. A system tends to resonate when the system is subjected to a force having a frequency coinciding with the system's natural frequency. Nevertheless, the system can have additional resonance frequencies different from the natural frequency. A mode shape tells how the structure vibrates at the specific natural frequency; every mode shape is unique [50]. Knowledge about the mode shapes can be advantageous when designing structures, the designer can modify the structure to increase or decrease the response [50].

If a system is described by its state space representation (equations (14) and (15)), the eigenvectors and eigenvalues of the $\boldsymbol{A}$ matrix corresponds to the mode shapes and the natural frequencies of the system [51]. The number of eigenvector and eigenvectors will be equal to the degrees of freedom of the system. A system oscillating without damping will have an undamped natural frequency [rad/s] which is calculated from the eigenvalue as [51]

$$\boldsymbol{\omega_n} = |\boldsymbol{\lambda}|$$

where || denotes the complex norm. Moreover, a system oscillating with damping will have a damped natural frequency considering a damping term as well. The damped natural frequency [rad/s] is calculated as [51]

$$\omega_d = \omega_n\sqrt{1-\zeta^2}$$

where ζ is the damping term and calculated as

$$\zeta = \begin{cases} 0, & if\ |\lambda| = 0 \\ \dfrac{Re(\lambda)}{|\lambda|}, & otherwise \end{cases}$$

The mode shape corresponding to the lowest frequency is referred to as the first mode shape, the mode shape related to second lowest frequency as the second and so forth [50].

4. Results

Firstly, the results for the explorations of forced oscillation in surge and heave are presented. The results of the forced oscillation are compared to operating cases to investigate whether the WEC's performance is affected by resonance in surge. In this thesis, an operating case refers to a simulation where the WEC system is not restricted to any motion. Thereafter, the results of the linearization including the eigenvalue and eigenvector analysis are presented. To clarify the presentation of the results, the period associated with surge motion is referred to as *oscillation period* and the period associated with heave motion is referred to as *wave period*. The figures demonstrating the distance of the buoy's oscillations are normalized due to confidentiality reasons and do only demonstrate the ratio between the magnitudes. The maximum value is represented as 1. The normalization does not affect the results or the later discussion.

4.1 Forced oscillation

4.1.1 Forced oscillation in surge

In Figure 17 the root mean square (RMS) value of the buoy motion from its equilibrium is shown when the excitation force is dominant and solely restricted to surge. The distance is represented in RMS values since it demonstrates an accurate average value of an oscillatory motion. The results indicate that the buoy's resonance frequency in surge depends on the magnitude of the excitation force, the oscillation periods corresponding to the resonance peaks increase for larger excitation magnitudes as well do the resonance bandwidths. The resonance peaks occur at 15.1 s, 16 s and 17 s for 1,000 N, 20,000 N, and 40,000 N, respectively. For the larger magnitudes, 20,000 N and 40,000 N, the heave motion is also increased for oscillation periods coinciding with the resonance although the buoy is only excited in surge.

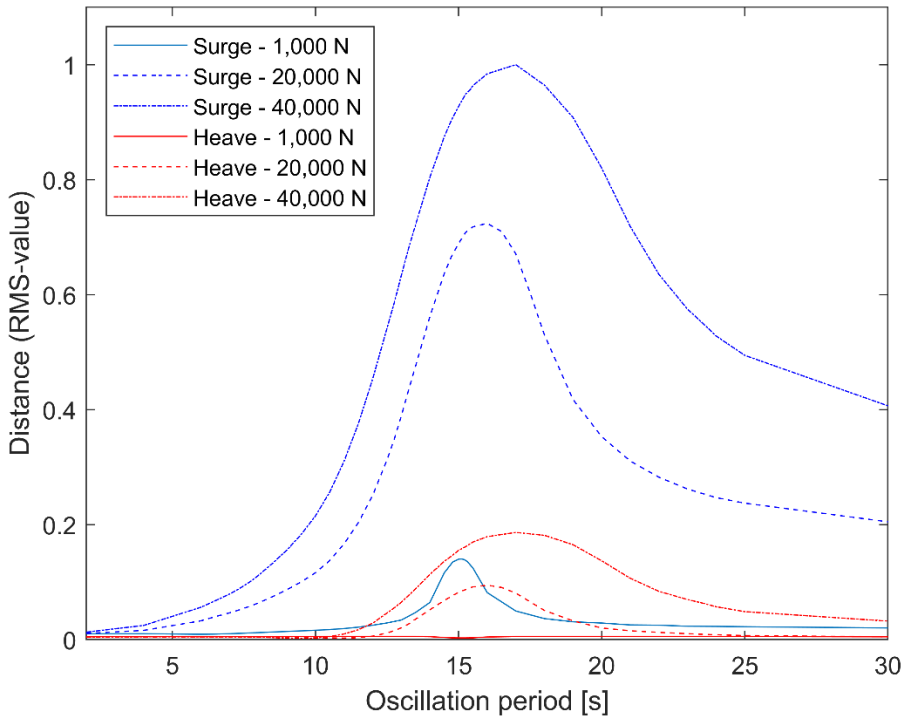

Figure 17. Forced oscillation in surge. Normalized motion of the buoy for different oscillation periods ranging from 2 - 30 s.

The surge motion is considerably amplified even for a small excitation force in surge, indicating a significant responsive system at that oscillation period. Figure 18 shows the time series of the surge motion for the resonance peak period of 15.1 s for the 1,000 N case. The motion is progressively amplified throughout the simulation indicating a resonance frequency for the oscillation period of 15.1 s and a forced oscillation in surge with magnitude 1,000 N.

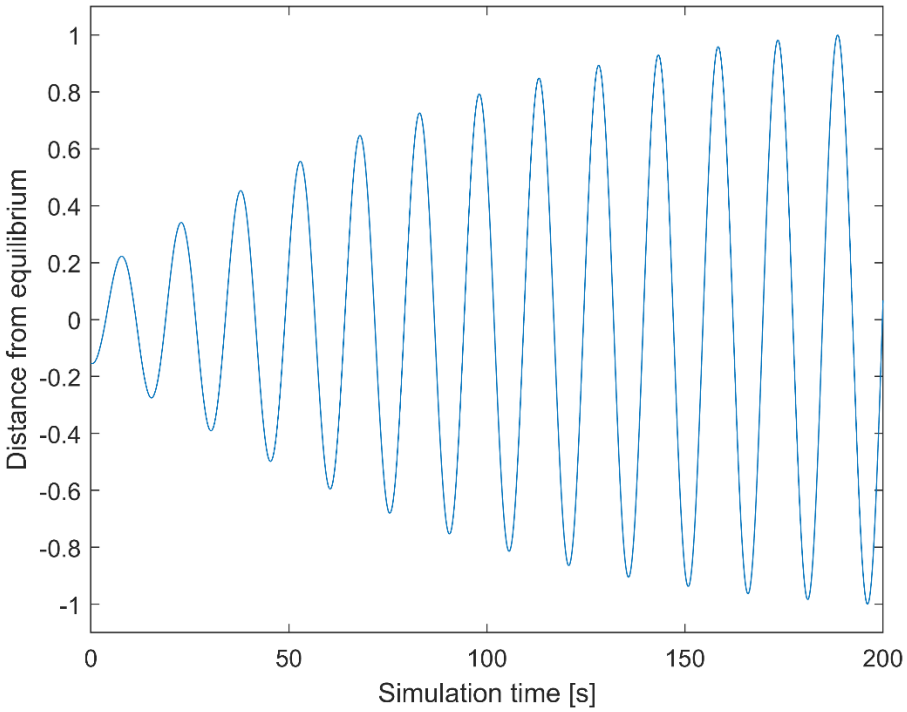

Figure 18. Normalized time series of the distance the buoy moves in surge at oscillation period 15.1 s when the excitation force is solely restricted to surge and has an amplitude of 1000 N.

4.1.2 Forced oscillation in heave

The results of the distance the buoy moves when the excitation force is solely restricted to heave are shown in Figure 19. In comparison to the results of forced oscillation in surge, there are no clear resonance peaks for the dominant excitation motion in heave. There is a wider peak with maximum at wave periods 10-11.5 s for all the three cases with excitation forces ranging from low to high. There is no surprise that there are no clear peaks in heave, the WEC is controlled to amplify the heave motion to maximize the energy performance. Moreover, the WEC is also designed to have a low natural frequency in heave not likely to coincide with the typical wave climate avoiding sharp resonance peaks in the device's heave response.

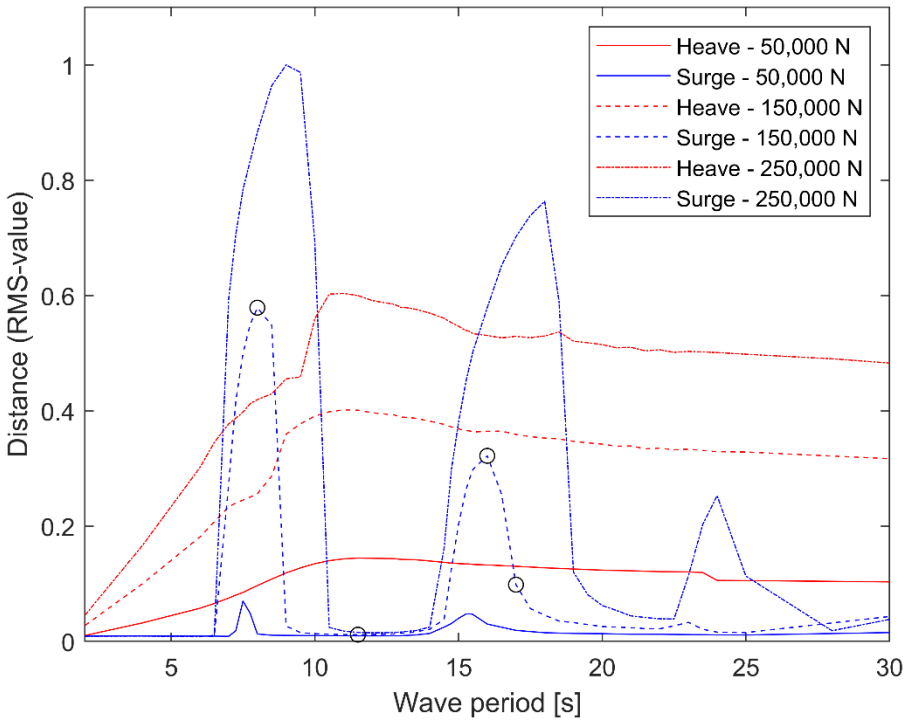

Figure 19. Forced oscillation in heave. Normalized motion of the buoy for different wave periods ranging from 2 – 30 s. The black circle corresponds to the wave periods demonstrated in Figure 20 and table 1.

However, there are two significant resonance peaks in the surge motion for all three cases when the WEC is solely excited in the heave mode. Two resonance peaks occur at wave periods 7.5 s and 15.4 s for the 50,000 N case, at wave periods 8 s and 16 s for the 150,000 N case, and at wave periods 9 s and 18 s for the 250,000 N case. The resonance peaks occur at higher wave periods for larger excitation forces, as well do the resonance bandwidths increase for larger wave loads. Additionally, for larger excitation forces, there are additional resonance peaks at wave periods between 23-25 s. However, these peaks are not as significant compared to the peaks at the lower wave periods. The common wave periods for the planned ocean sites are usually below 14 s and the typical wave is characterized by having $t_p = 8 - 10.5\,s$. Since the excitation in heave is strongly coupled to the oscillation of the incident wave, the first resonance peak imply that the buoy will resonate in surge for the many of the typical sea states.

Figure 20 illustrates four time series of the surge motion for the 150,000 N case at wave periods 8 s, 11.5 s, 16 s and 17 s, these surge responses are demonstrated by a black circle in Figure 19. As indicated in Figure 19, there are resonance in surge at wave periods 8 s and 16 s, the surge motion is for these two wave periods significantly amplified. Table 1 demonstrates the oscillation periods, the time between the surge peaks in Figure 20, and the resonant wave periods of 8 s and 16 s have the similarity of having oscillation periods around 16-16.1 s. The oscillation periods indicate that the surge resonance peak occur at its maximum when the surge motion of the buoy have a

period close to 16.1 s for a restricted excitation force in surge of 150,000 N. In comparison, at wave period 11.5 s where there is no resonance, the oscillation periods are more varying and do not coincide with the peak resonance period of 16.1 s. Furthermore, at wave period 17 s the surge motion is greater than for wave period 11.5 s but smaller than for wave periods 8 s and 16 s. The oscillation periods for wave period 17 s are slightly greater than the peak oscillation period of 16.1 s. Nevertheless, the oscillation periods for wave period 17 s seem to be within the surge mode's resonance bandwidth still amplifying the surge motion.

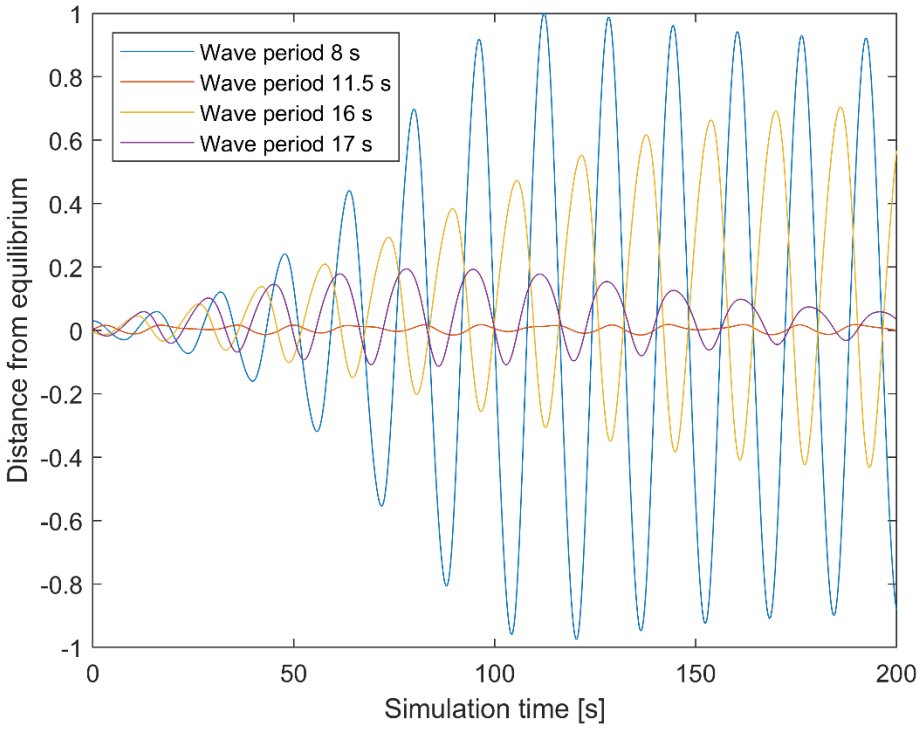

Figure 20. Normalized distance from equilibrium in surge when a forced heave oscillation is applied as excitation force with an amplitude of 150,000 N and periods 8 s, 11.5, 16 s and 17 s.

Table 1. Oscillation periods [s] in surge for the time series in Figure 20 and the corresponding marked wave periods in Figure 19.

t = 8 s	t = 11.5 s	t = 16 s	t = 17 s
15.90	13.70	15.30	16.10
16.00	19.00	15.60	16.30
16.00	14.05	15.75	16.45
16.10	13.50	15.85	16.55
16.20	19.10	15.90	16.55
16.20	14.10	16.05	16.60
16.05	18.85	16.05	16.65
16.05	13.75	16.10	16.65
16.00	14.05	16.10	16.75
16.00	18.70	16.15	16.95
16.00	14.00	16.10	17.60
	13.90		

To summarize, resonance in surge seems to appear when the incident wave has a wave period around 6.5-10.5 s and 13.5-19 s. However, the WEC is not likely to resonate with wave periods around 13.5-19 s since these sea states are rare. Larger wave loads results in wider resonance bandwidths. At the resonant wave periods, the surge motion of the buoy tends to oscillate around the surge mode's resonance frequency presented in 4.1.1 Forced oscillation in surge resulting in an amplified surge motion.

4.1.3 Operating cases

Figure 21 shows four operating cases characterized by incident waves of different heights. Although the WEC in operation is most likely subjected to smaller wave periods, Figure 21 demonstrates wave periods up to 30 s. Such high wave periods are extremely unlikely, however, there are included in this results to examine whether there are any trends in how surge resonance is affecting the performance of the WEC.

The results from forced oscillation in heave, Figure 19, resemble the real operating cases. The three lower incident waves confirm that the buoy is the most resonant at two intervals at wave periods around 7-9.5 s and 14-21 s. However, the highest operating case defined by an incident wave with height $H = 3.75\,m$ does not have as clear resonance peaks but shows a more general amplified surge motion for wave periods up to 20 s. The forced oscillation results indicated that the greater magnitude the excitation force have, the broader the resonance bandwidths in surge becomes.

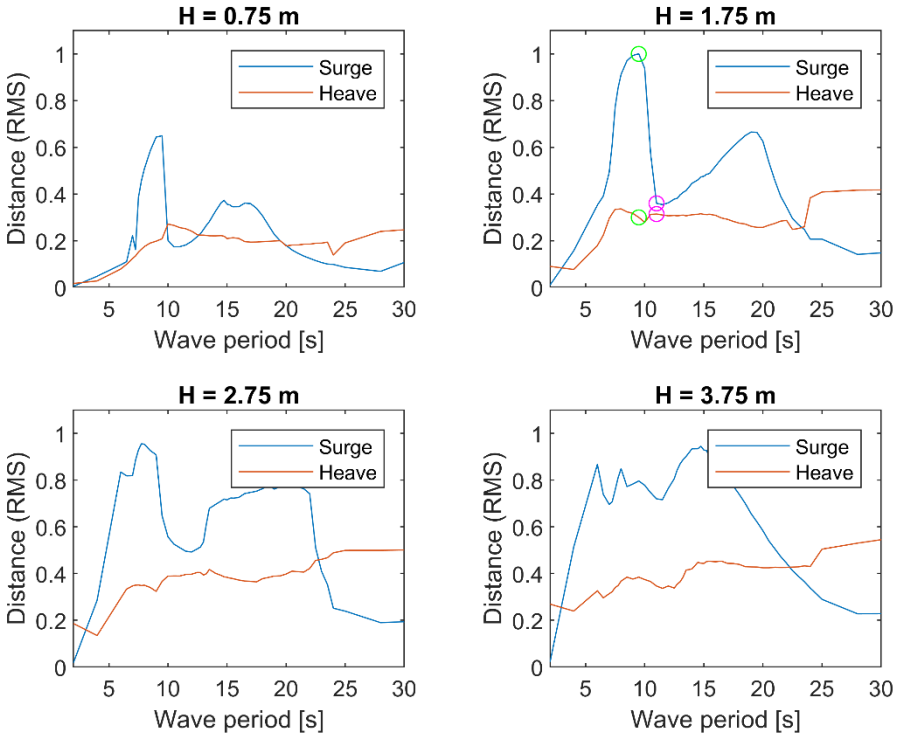

Figure 21. Normalized motion of four operating cases defined by different wave heights of the incident wave. In the $H = 1.75\ m$ plot, the green and the magenta colored circles represents the motion for $t = 9.5\ s$ and $t = 11\ s$, respectively.

All four operating cases show tendencies that the heave motion is affected by resonance in surge. The heave motion stabilizes and reaches its maximum for wave periods equal or larger than 25 s. The typical wave periods at the Aguaçadoura location, $t_p = 8 - 11.5\ s$, seem to have a restrained heave motion. The heave motion seems to be limited when the surge motion is relatively large. Consequently, since the PTO system converts the relative heave motion to electricity, the implication of the restrained heave motion is that the energy production of the WEC system will be negatively affected by resonance in surge.

Figure 22 illustrates two time series of the heave and the surge motions for the operating case characterized by an incident wave with height $H = 1.75\ m$ (upper right plot in Figure 21). The upper plot in Figure 22 represents the motions for $t = 9.5\ s$, when resonance in surge occurs (green colored circles in Figure 21). The lower plot represents the motion for $t = 11\ s$, when there is no resonance in surge (magenta colored circles in Figure 21). The two time series demonstrate a scenario where an amplified surge motion affects the productive heave motion. When the WEC is resonant in surge the heave motion follows an oscillatory pattern, but the motion is for every second oscillation reduced to half. In contrast, when the buoy is non-resonant in surge the heave motion is not limited but follows a smooth sinusoidal pattern. Compared to the non-resonance case, $t = 11\ s$, the buoy at surge resonance, $t = 9\ s$, is at a surge position further away from its equilibrium restricting the buoy from going below the

mean water level. For every second heave oscillation the relative heave motion is reduced to half implicating the energy performance will be lower when resonance in surge occurs compared to a non-resonant oscillation.

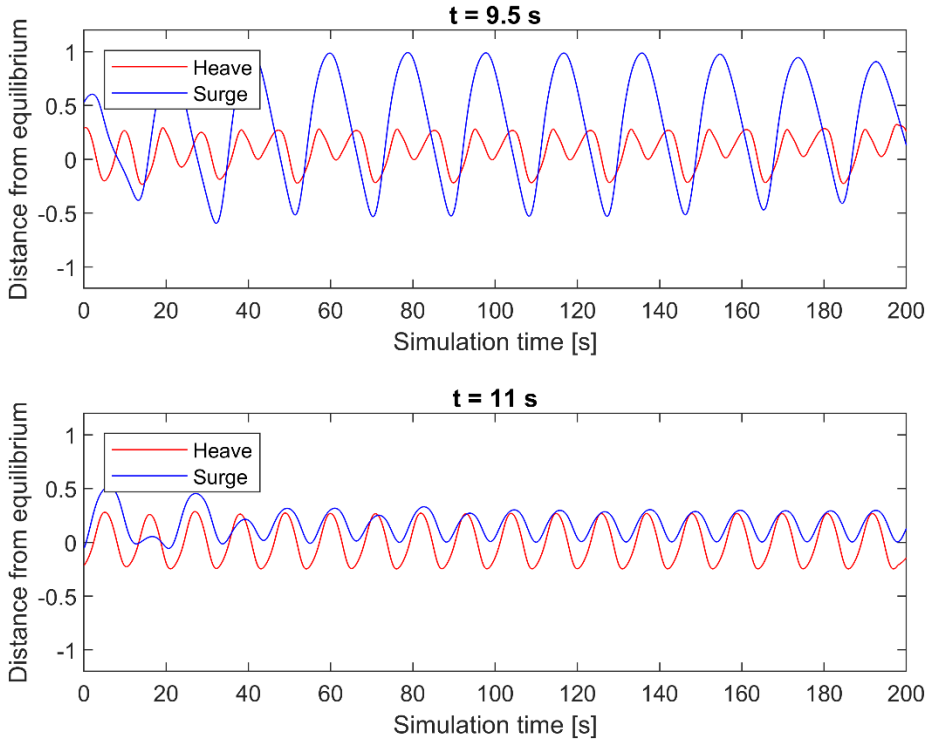

Figure 22. Normalized time series demonstrating the ratio between the heave motion and the surge motion for wave periods $t = 9.5\ s$ and $t = 11\ s$ for the operating case with an incident wave with wave height $H = 1.75\ m$.

4.2 Linearization

Figure 23 shows bode plots of four linearized systems of the WEC characterized by incident waves having various wave periods and wave heights. The systems were linearized at the initial simulation time, $t_s = 0\ s$, meaning the incident wave had just started. However, the height of the incident wave was much smaller than the height indicated in the plot's legend since the model ramps up the wave height during the first ten seconds to avoid shocks. A fully developed wave is not represented in the presented plots as an operating point based on higher simulation times, in general, did not generate as adequate bode plots as operating points close to the initial time, this will later be discussed in 5.1.3 Linearization. The four bode plots have resonance peaks around the same wave periods for the operational sea states, in the interval of 0.42-0.77 rad/s (14.80-8.19 s). Resonance in the bode plots are indicated by the peak in the magnitude plot as well as the phase shift of 90 degrees of the motion in relation to the excitation force meaning the velocity is in phase with the incoming wave. However, the bode plots do not resemble each other entirely. This is not surprising since a WEC is a dynamical system without a steady state and different incident waves will have different

impacts on the WEC since they constitute different magnitudes of the force acting on the buoy.

As mentioned in section 3.4 Linearization, if a system is linearized at an arbitrary state and not at a steady state, results of the linearization should be compared with an accurate nonlinear simulation of the system. Linearization of the WEC system does not restrict any motion of the buoy but it is possible to study the characteristics of the system in a regular operating mode. In an operating mode, the WEC system is designed to amplify its heave motion, for that reason, the results of the linearization should be compared to the results of the forced oscillation in heave and not to the results of forced oscillation in surge. The linearized system that most resembles the nonlinear system is the system defined by an incident wave characterized by $t = 9\,s$ and $H = 1.75\,m$. Compared to the results of the forced oscillation in heave and the operating cases, this system also has two clear resonance peaks at 0.430 rad/s (14.605 s) and 0.767 rad/s (8.19 s) and the highest frequency peak of the two is the greatest one. For these reasons, the system that hereafter will be regarded in the eigenvalue and eigenvector analysis is the system defined by an incident wave with $t = 9\,s$ and $H = 1.75\,m$. However, worth noting is that none of the linearized systems have any resonance peak at higher wave periods as indicated by the earlier presented results.

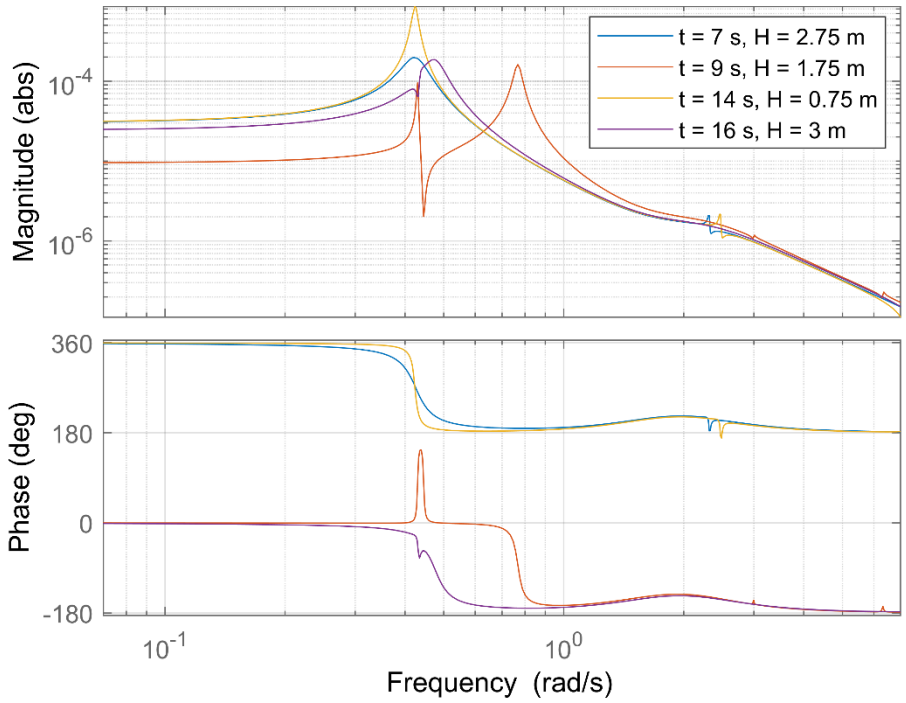

Figure 23. Bode plot of the WEC system with four different incident waves. The WEC systems were linearized at the initial simulation time.

Figure 24 shows the WEC system in the sea state of $t = 9\ s$ and $H = 1.75\ m$ linearized at various simulation times. Although the operating points are close to each other in simulation time, the bode plots of the linearized systems differ, indicating a time variant system and a non-steady state as operating point. Moreover and as touched upon, when linearizing the WEC system, operating points based on simulation times close to the initial time generated, in general, adequate bode plots as the bode plots in Figures 23 and 24. However, when the WEC system, defined by the same sea state, was linearized at higher simulation times, the results of those linearizations did in most cases, generate uncharacteristic bode plots not capturing the known dynamics of the system. The system linearized at simulation time $t_s = 2\ s$ is illustrated in Figure 25, note the changed axes compared to the previously presented bode plots.

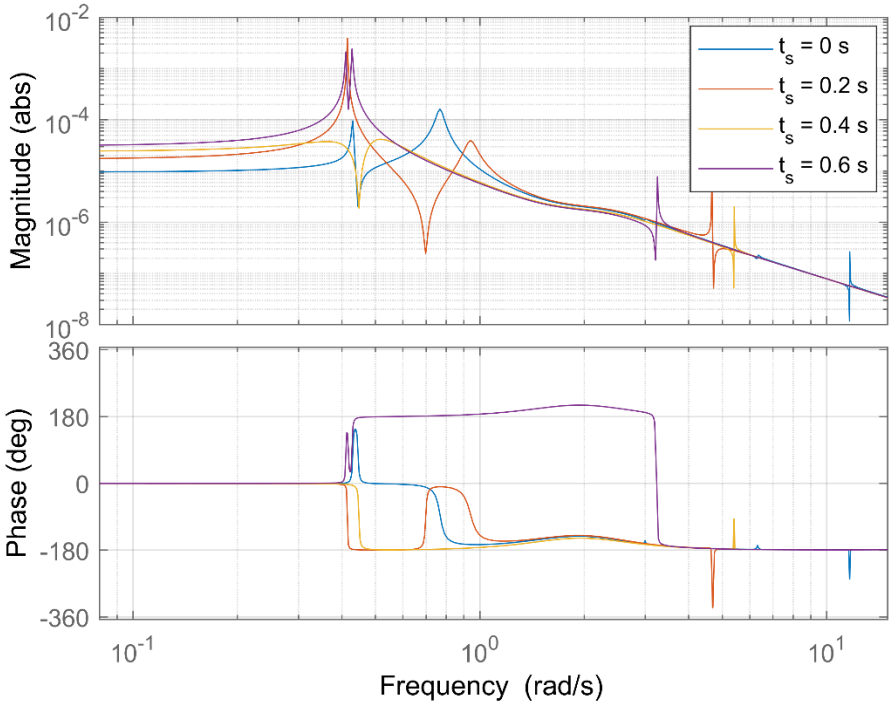

Figure 24. Bode plot of linearized systems defined by $t = 9\ s$, $H = 1.75\ m$ and linearized at various simulation times, t_s, as operating point.

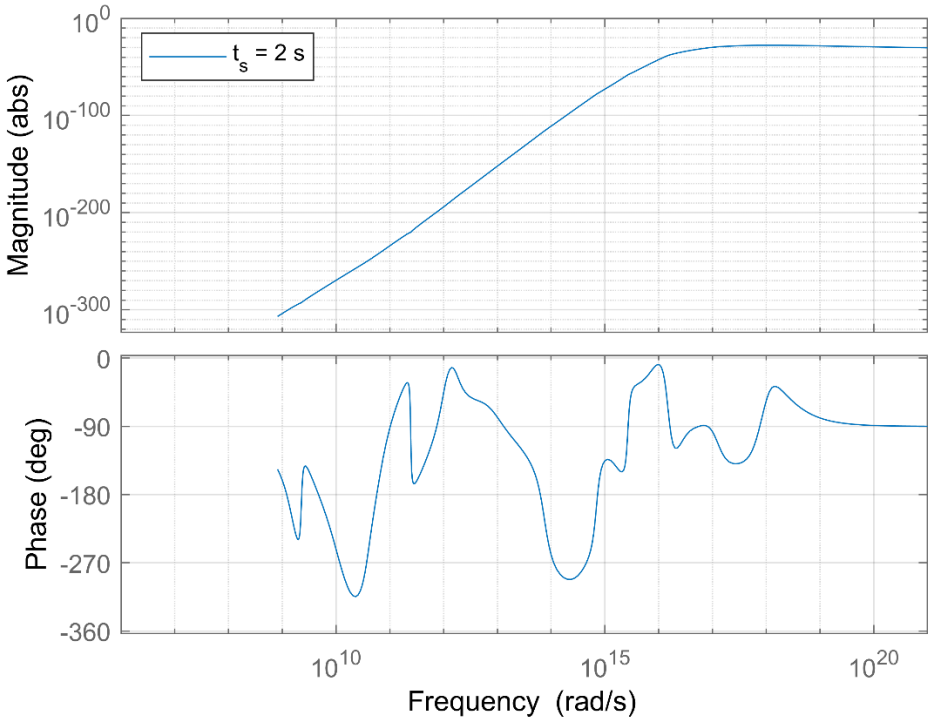

Figure 25. Bode plot of the system characterized by an incident wave with $t = 9\ s$, $H = 1.75\ m$ and operating point at simulation time $t_s = 2\ s$. Note the changed axes compared to the previous bode plots.

4.2.1 Eigenvalue and eigenvector analysis

The outcome of the system linearized at the initial simulation time, $t_s = 0\ s$, with an incident wave characterized by $t = 9\ s$ and $H = 1.75\ m$ was a state space representation with 169 states, including states from the PTO block, the hydrodynamic block, and the mooring block, see appendix A. Most of the states were complex conjugated. The eigenvalues and their corresponding mode(s) and wave period(s) are shown in Table 2 for eigenvalues having a wave period in the range of $t = 1 - 50\ s$. The two biggest resonance peaks in the system's bode plot at 0.7675 rad/s (8.1824 s) and 0.4301 rad/s (16.6013 s) are natural frequencies to the WEC system meaning that they occur due to the structure of the system. In the bode plot, there are also two smaller resonance peaks at 2.9961 rad/s (2.0961 s) and 6.3206 rad/s (0.9936 s) also being natural frequencies. What all these four eigenvalues have in common in comparison to the other eigenvalues in Table 2 is that the real part of the eigenvalue is positive or close to zero. The other eigenvalues can be assumed to have more damping to their respective mode shape and can be considered more stable.

Table 2. Modes, eigenvalues, and wave periods in sea states with $t = 1 - 50\ s$.

Mode(s)	Complex eigenvalue(s)	Wave period [rad/s]	Wave period [s]
⋮	⋮	⋮	⋮
7, 8	$0.0021 \pm 0.4301i$	0.4301	14.6013
9	-0.4719	0.4719	13.3079
10, 11	$-0.6231 \pm 0.5162i$	0.5162	12.1658
12, 13	$-0.0185 \pm 0.7675i$	0.7675	8.1824
14, 15	$-0.6271 \pm 1.0959i$	1.0959	5.7304
16	-1.3411	1.3411	4.6827
17, 18	$-0.5422 \pm 1.3501i$	1.3501	4.6515
19, 20	$-0.5422 \pm 1.3503i$	1.3503	4.6508
21	-1.4392	1.4392	4.3635
22	-1.4939	1.4939	4.2038
23, 24	$-1.0479 \pm 1.8129i$	1.8129	3.4641
25, 26	$-0.9707 \pm 2.0536i$	2.0536	3.0580
27, 28	$-0.9367 \pm 2.1291i$	2.1291	2.9543
29, 30	$-1.4127 \pm 2.2320i$	2.2320	2.8136
31, 32	$-1.4081 \pm 2.2351i$	2.2351	2.8097
33, 34	$-0.0085 \pm 2.9961i$	2.9961	2.0961
35, 36	$-0.0311 \pm 6.3206i$	6.3206	0.9936
⋮	⋮	⋮	⋮

The eigenvectors corresponding to complex conjugated eigenvalues were also complex conjugated. The eigenvector for the eigenvalues $0.0021 \pm 0.4301i$ and $-0.0185 \pm 0.7675i$ are found in appendix A together with operating state values at the same simulation time. In general, the eigenvectors were small and significantly smaller than the operating state values, the states had usually an exponent less than –5. The eigenvectors corresponding to the two highest resonance responses were simply ocular analyzed by comparing the real parts of the eigenvectors to operating values of the included states. Investigation of the two eigenvectors showed that parts of the mooring system had tendencies of being significantly higher than the other states in relation to normal operating values. More specifically, the part of the mooring system that showed tendencies of affecting the device response was the mooring buoy ("Mooring buoy dist." and "Mooring buoy vel." in Appendix A). Previously, the WEC was designed to have a bigger submerged mooring buoy as a part of the mooring system. However, the mooring buoy is no longer a part of the WEC design, but the mooring buoy is still

represented in the model as a small buoy with diameter 1 m and height 1 m. The implications of the eigenvector analysis were further investigated by simulation with variations of the structure of the mooring system.

Figure 26 shows bode plots of three systems, one with the default mooring system detailed for above, and the other two having a smaller mooring system as well as a bigger mooring system. More specifically, the dimensions of the mooring buoy were changed, for the small mooring system the mooring buoy diameter and height were set to 0.01 m and 0.01 m, respectively, and for the bigger mooring system the mooring buoy diameter and height were set to 5 m and 5 m, respectively. The smaller mooring buoy is not a realistic size of the buoy, the purpose of the having such a small size was to examine whether the mooring buoy impacted the frequency response. The resonance responses were shifted by changing the structure of the mooring system of the WEC. The dominant force affecting the response of the submerged mooring system is the drag force. The drag force in turn is dependent on the projected area facing the direction of the motion. Therefore, shifting the drag area should affect the mooring response, and further, depending on the system characteristics, the mooring system might affect the overall device response of the WEC. However, forced oscillation in heave and operating case simulations did not confirm the results of the eigenvector analysis that the mooring system is causing the resonance responses. Figure 27 shows the results of forced oscillating in heave and operating case simulations with a smaller mooring system as well as the default mooring system. The results of the default mooring buoy are demonstrated by the blue curve for the surge response and the red curve for the heave response. The results of the smaller mooring buoy are demonstrated by the yellow curve for the surge response and the purple curve for the heave response. Figure 27 is indicating that there is almost no difference between the two mooring systems, the yellow and purple curves are on top of the blue and red curves. The simulations have insignificantly deviations to each other, consequently, the mooring buoy does not seem to affect the resonance as indicated by the eigenvector analysis.

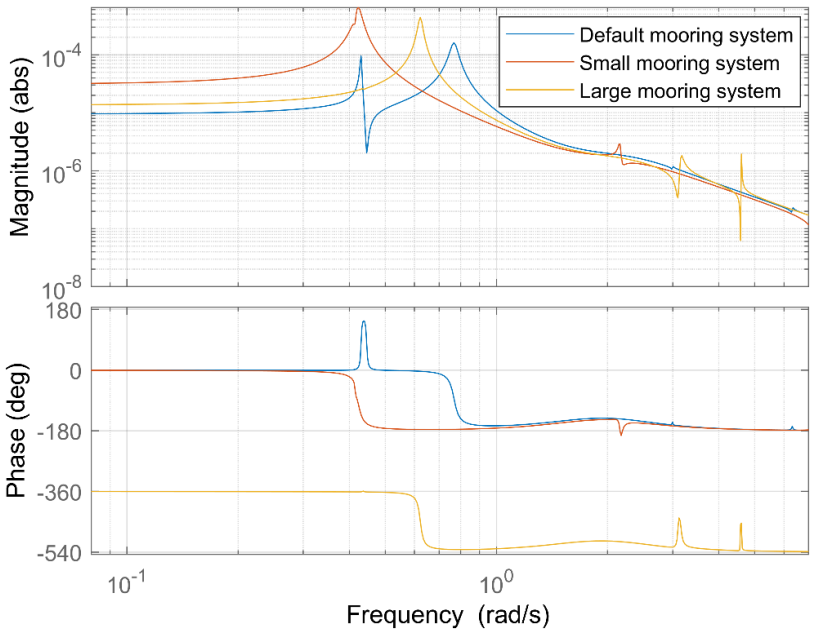

Figure 26. Bode plots of the WEC with three different mooring systems.

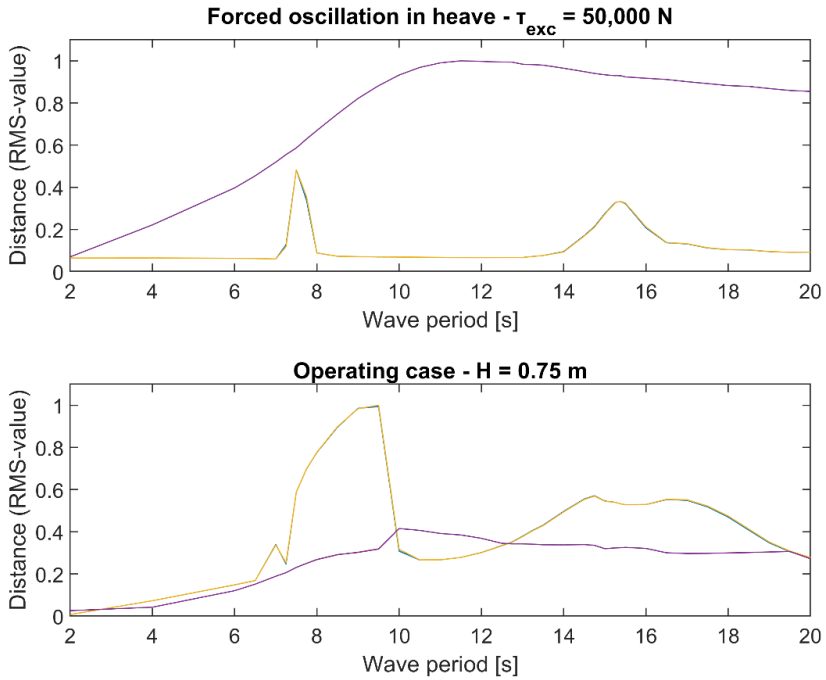

Figure 27. Normalized simulations with a regular mooring system and a smaller mooring system for the forced oscillation in heave scenario and the operating case. The results of the regular mooring buoy are illustrated by the blue curve for the surge response and the red curve for the heave response. The results of the smaller mooring buoy are represented by the yellow curve for the surge response and the purple curve for the heave response.

5. Discussion

The discussion section elaborates the evolved consequences of the assumptions as well as analyzes the strengths and the weaknesses of the methods. Accordingly, the section aims at highlighting the results in a bigger perspective. Lastly, the section proposes future studies.

5.1 Discussion of assumptions and methods

5.1.1 Assumption of regular wave

The waves in the ocean are of changing character, therefore, the assumption of regular waves is a simplification that is not compatible with the reality. Simulation with regular waves allows the buoy to settle its motion response to the specific wave climate. However, a buoy floating in the ocean does most likely not settle its response to the wave climate since the wave climate is ever changing. The buoy will in its operational state be subjected to different wave frequencies. This elucidation indicates that the progressive amplification of the motions in Figures 18 and 20 demonstrate a scenario that may be an overestimate of the reality implying that the surge resonance would have smaller impacts. Nevertheless, the results indicate that the resonance bandwidth includes the most typical sea states, $t_p = 8 - 10\ s$, indicating that although the buoy will not be subjected to its peak resonance frequency in surge, it will for common periods still be affected by an amplified motion in surge. Furthermore, the implication of the results is that the heave motion is affected by the resonance in surge. Therefore, it is probable that during a more realistic scenario of irregular waves, the energy performance will still be affected by the buoy's resonance in surge.

5.1.2 Forced oscillation

A limitation with the forced oscillation method is that the simulation does not resemble an operational scenario, but rather a restricted system. A consequence of this fact is that it is difficult to draw any conclusions to which operational scenario for instance a sole excitation force in surge of 20,000 N corresponds to. Therefore, the results give hints at what frequencies resonance occur but not the exact situations when resonance occurs. When comparing the results of the forced oscillation in heave, Figure 19, to real operating scenarios, Figure 21, the forced oscillation method seems to represent the system quite well and the results gives a good overview over the system characteristics.

A disadvantage with the forced oscillation method is that the results do not contain any information about what parts of the system that are causing the resonance. Because of the complexity of the system, it is difficult to make an educated guess what instigates the resonance peaks. With regards to the origin of the resonance, linearization is a preferrable method, however, the confidence of the linearization results seems to be low.

5.1.3 **Linearization**

Utilizing the method of linearizing could be an advantageous tool in the development of WECs. Models of WEC systems are often complex, as the model this thesis is based on illustrates, consequently, it can be difficult to isolate smaller components of the system and investigate their respective characteristics. Therefore, linearization can be an important tool since it is possible to isolate smaller systems with regards to inputs and outputs of interest. The investigation in this thesis was limited to the buoy of the WEC and its system characteristics could be found with an alternative method of forced oscillation, however, for other components it could be more difficult to "force" an oscillation and isolate the system as the coupling between the different parts of the WEC structure is complex. Information about the characteristics of smaller components of the full system gives the designer valuable knowledge how a part of the system responds to certain frequencies and affects the whole system. However, it seems to be difficult to ensure the credibility of linearization of nonlinear complex systems.

WECs are dynamic systems with no steady state, the characteristics of WECs are oscillatory and involves large forces and advanced control strategies to increase the energy performance. Therefore, as mentioned in the results, it is not unexpected that the linearization results are time variant. However, the results raise concerns regarding how time variant a WEC system is expected to be and why the linearization results seem adequate for operating point close to the initialization of the simulation. For the reasons of complexity described for above, it is difficult to investigate what causes what in the WEC, metaphorically speaking it is difficult to understand which responses that are the chicken and which responses that are the egg. Therefore, it is challenging to evaluate the credibility in the linearization results. Ljung and Glad argued [47] that it is difficult to quantitively estimate how accurate the linearization is, and the results in this thesis implicate just that. Consequently, Ljung and Glad further reasoned that the results of a linearization shall be carefully treated. The linearization results were compared to operating cases as well as the forced oscillation results since forced oscillation showed good resemblance to the operating cases. The bode plots having operating points based on simulation snapshots proximate to the initializing of the simulation and characterized by different wave periods and wave heights showed all at least one resonance peak in the wave period interval of 6 – 15 s as expected from the operating cases. Nevertheless, there were significant variations for small changes in choice of operating point as well as wave period and wave height of the incident wave and the question is whether this is expected or not.

It is still not known why the linearization generally worked for simulation times close to the initial state. To this day, the linearization tool has, for CorPower Ocean's Simulink model, the character of being a black box. MathWorks, the developer of MATLAB and Simulink, offers an advisor tool aiming at evaluating and, if necessary, troubleshooting the results of the linearization [48]. However, despite several tries and approaches, the advisor tool did not work on the WEC model. MathWorks states [48] that there are

some Simulink blocks that have the property of linearizing poorly, for instance, there are some blocks not having a defined Jacobian generating poorer result, operating points near discontinuities usually perform inadequate result and event-based subsystems can also be a reason for poor results. One guess could be that the system at the simulation times not generating sufficient linearizations involve discontinuities in the system originating from the control block regulating the device response.

As elucidated, the linearization in this thesis investigation seemed to, generally, perform more adequate results for early simulations times as operating points. What the systems have in common at early simulation times, irrespective of wave period and wave height, is that the wave height is restricted and ramped up during the first ten seconds resulting in small hydrodynamic forces. Consequently, the linearization might be sensitive to high forces. Big forces, in turn, might be coupled to a regulator in the control system and so forth. However, without having a sufficiently good understanding on how the linearization is performed, it is difficult to analyze the different results. Using another metaphor, to manually investigate what causes different linearization results is like looking for a needle in a haystack. In general, the model is too complex to, in a thoroughly and hierarchical way, investigate in what way the blocks in the full Simulink model are coupled to each other.

Although the credibility of the linearization is uncertain and can be considered low, the eigenvalue and eigenvector analysis could still be an advantageous tool. Provided that the linearization result is sufficiently accurate, the eigenvalues contain information about the system's natural frequencies. As mentioned, the natural frequencies are solely dependent on the structure of the system and knowledge about them are valuable. Although the characteristics of the bode plots in Figures 23 and 24 varied, all the bode plots had resonance peaks and corresponding natural frequencies for wave periods between 8.19-14.8 s, indicating that buoy have tendencies to be resonant around those frequencies. The WEC designer can with this knowledge about the eigenvalues re-design the structure to dampen the resonant response if desired.

The interpretation of the eigenvectors is not as straightforward as the interpretation of the eigenvalues. In this thesis a simple comparative analysis between the eigenvector's state values and those state values during a normal operating case was done. The simple analysis implied that the resonance had its root cause in the mooring system which linearizations confirmed, however, forced oscillation and operating case simulations with a changed mooring system did not significantly affect the results compared to the default mooring system. Although the eigenvector analysis was unsuccessful in this thesis, it still concretized which specific parts and control systems of the WEC that impacts the motion response in the state space representation which is valuable knowledge. The analysis of the eigenvector was in these investigations merely ocular and can be considered shallowed, a more statistical developed analysis might provide more confident insights in what is causing the resonance. To sum up the eigenvalue and eigenvector analysis, provided that the credibility of the linearization is good enough, a

more statistical developed method of evaluating the eigenvectors might together with the eigenvalues, not only give knowledge when the system is resonant, but also what in the structure that causes the resonant response.

To summarize the discussion of the utilized methods, the forced oscillation method generated accurate results when the buoy is resonant in the surge mode. However, the forced oscillation method lacks the capability to explore what is causing the resonant response. The method of linearization, on the other hand, theoretically possesses the capability to investigate what in the structure that cause resonance. However, the credibility of the linearization method seems for a non-linear and dynamical WEC system to be low, and consequently, the low credibility might impact the methods capability to explore what is causing the resonance.

5.2 Future work

This thesis work has evoked further interesting aspects that could be emphasized in future studies associated with surge resonance in WEC systems.

As touched upon in the discussion, future work associated with surge resonance studies of a WEC would gain further knowledge if including a more realistic scenario of irregular waves. For this reason, future work should include irregular waves. Furthermore, the angle of incidence the buoy is hit by the incident wave does most likely also affect the device response of the WEC. Therefore, future studies should also include different angles of incidence and study their effects.

As discussed, linearization has the potential to be a valuable tool in the development of WECs, however, today the method has not enough credibility. Therefore, future work regarding device resonance responses in WECs should concern how linearization approaches on highly dynamical and nonlinear system, such as WECs, can be made more transparent and credible. Moreover, if the linearization method is shown to have a sufficiently credibility, future studies should develop statistical methods investigating the eigenvectors. These studies should highlight the question when a state in an eigenvector can assumed to be a significantly instigator to the corresponding eigenvalue and resonance response.

In this thesis the implication was made that surge resonance impacts the energy output performance of the WEC since the heave motion is negatively affected by the surge resonance. However, the investigation has not quantitatively assessed the effect on the energy output performance. A quantitative estimate would give further insights in whether it is economical beneficial to reduce the surge resonance or if it costs more than the kilowatt hours earned. Therefore, interesting aspects in a future study associated with surge resonance are inclusion of quantitatively estimation of the energy performance.

6. Conclusions

Surge resonance occurs in CorPower Ocean's WEC when the buoy has an oscillation period in surge of 15-17 s. The peak and the bandwidth of the resonance are dependent on the magnitude of the excitation force, larger wave loads results in higher resonance peak periods and larger bandwidths. Furthermore, surge resonance occurs when the incident wave oscillates with periods of 6.5-10.5 s and 13.5-19 s. However, the WEC in the planned sites will be prominently subjected to periods in the interval 8-11.5 s, thus, it is unlikely that surge resonance above these wave periods will occur. In conformity with the surge oscillation resonance, the peaks and the bandwidths of the resonance are dependent on the magnitude of the excitation force.

The results indicate that the heave motion response is negatively affected by resonance in surge. The implication of that is that the annual energy output is negatively affected as well since the PTO system of the WEC utilizes the emerged relative heave motion. The investigation have not been able to find an answer on how the surge resonance should be mitigated. The results of one of the two utilized methods, linearization, showed tendencies that parts of the mooring system was the instigator to the surge resonance. However, the other method, forced oscillation, as well as operating cases did not confirm that the mooring system causes the resonance in surge.

References

[1] Gunn, K. Stock-Williams, C. 2012. Quantifying the global wave power resource. *Renewable Energy*. 44, 296-304.

[2] International Energy Agency. 2020. Data and statistics. https://www.iea.org/data-and-statistics?country=WORLD&fuel=Energy%20consumption&indicator=TotElecCons (2020-09-16)

[3] Falnes, J. 2007. A review of wave-energy extraction. *Marine Structures*. 20, 185-201.

[4] Ringwood, J. Bacelli, G. Fusco, F. 2014. Energy-maximizing control of wave-energy converters. IEEE Control systems magazine. October 2014, 30-55.

[5] Engström, J. Kurupath, V. Isberg, J. Leijon, M. 2011. A resonant two-body system for a point absorbing wave energy converter with a direct-driven linear generator. *Journal of Applied Physics*. 110:124904.

[6] CorPower Ocean AB. 2019. Commercial projects. https://www.corpowerocean.com/projects/ (2020-09-02)

[7] CorPower Ocean AB. 2019. *Technology*. https://www.corpowerocean.com/technology/ (2020-09-04)

[8] Falnes, J. Hals, J. 2012. Heaving buoys, point absorbers and arrays. *Philosophical Transaction of the Royal Society A.* 370, 246-277.

[9] Al Shami, E. Wang, X. Zhang, R. Zuo, L. 2019. A parameter study and optimization of two body wave energy converters. *Renewable Energy*. 131, 1-13.

[10] Haraguchi, R. Asai, T. 2020. Enhanced power absorption of a point absorber wave energy converter using a tuned inertial mass. *Energy*. 202, 117740.

[11] Sakr, A. Anis, Y. Metwalli, S. 2015. System Frequency Tuning for Heaving Buoy Wave Energy Converters. In: *IEEE International Conference on Advanced Intelligent Mechatronics (AIM)*. Busan, Korea July 7-11, 1367-1372.

[12] Ding, B. Sergiienko, N. Meng, F. Cazzolato, B. Hardy, P. Arjomandi, M. The application of modal analysis to the design of multi-mode point absorber wave energy converters. *Ocean Engineering*. 171, 603-618.

[13] Meng, F. Ding, B. Cazzolato, B. Arjomandi, M. Modal analysis of a submerged point absorber with asymmetric mass distribution. *Renewable Energy*. 130, 223-237.

[14] CorPower Ocean AB. 2019. About us. https://www.corpowerocean.com/about-us/ (2020-09-02)

[15] Drew, B. Plummer, A R. Sahinkaya, M N. 2009. A review of wave energy converter technology. *Proceedings of the Institution of Mechanical Engineers, Part A: Journal of Power and Energy*. 223, 887-902.

[16] Al Shami, E. Zhang, R. Wang, X. 2019. Point Absorber Wave Energy Harvesters: A Review of Recent Developments. *Energies*. 12:47.

[17] IPCC. 2014. Climate Change 2014: Synthesis Report. Contribution of Working Groups I, II and III to the Fifth Assessment Report of the Intergovernmental Panel on Climate Change [Core Writing Team, R.K. Pachauri and L.A. Meyer (eds.)]. IPCC, Geneva, Switzerland, 151 pp.

[18] Indra al Irsyad, M. Anthony Halog, A. Nepal, R. 2019. Renewable energy projections for climate change mitigation: An analysis of uncertainty and errors. *Renewable Energy*. 130, 536-546.

[19] Folley, M. 2017. The Wave Energy Resource. In Pecher Arthur and Kofoed Jens Peter (editors). *Handbook of Ocean Wave Energy*. Volume 7. Springer, 43-80.

[20] Sinha, A. Karmakar, D. Guedes Soares, C. 2016. Shallow water effects on wave energy converters with hydraulic power take-off system. *The International Journal of Ocean and Climate Systems*. 7:3, 108-117.

[21] Aqua-RET. 2012. Download Images and Illustrations. http://www.aquaret.com/indexea3d.html?option=com_content&view=article&id=203 &I temid=344&lang=en (2020-09-21)

[22] Yemm, R. Pizer, D. Retzler, C. Henderson, R. 2012. Pelamis: experience from concept to connection. *Philosophical Transactions of the Royal Society A*. 370, 365-380.

[23] BBC. 2014. Jobs go after no buyer found for Pelamis wave business. https://www.bbc.com/news/uk-scotland-scotland-business-30560980 (2020-09-11)

[24] Cameron, L. Doherty, R. Henry, A. Doherty, K. Van ’t Hoff, J. Kaye, D. Naylor, D. Bourdier, S. Whittaker, T. 2010. Design of the Next Generation of the Oyster Wave Energy Converter. I *EWTEC 2010: 3rd International Conference on Ocean Energy*. Bilbao, Spain 6 October.

[25] BBC. 2015. Jobs lost as wave energy firm Aquamarine Power folds. https://www.bbc.com/news/uk-scotland-scotland-business-34901133 (2020-09-10)

[26] Wave Dragon. 2017. About Us. http://www.wavedragon.co.uk/about-us/ (2020-09-10)

[27] Parmeggiani, S. Kofoed, J P. Friis-Madsen, E. 2013. Experimental Update of the Overtopping Model Used for the Wave Dragon Wave Energy Converter. *Energies*. 6, 1961-1992. doi:10.3390/en6041961.

[28] Wave Dragon. 2020. Specifications. http://www.wavedragon.net/specifications/ (2020-11-03)

[29] Wave Swell. 2020. Technology. https://www.waveswell.com/technology/ (2020-09-10)

[30] Wave Swell. 2020. King Island project. https://www.waveswell.com/king-island-project-2/ (2020-09-10)

[31] Wave Swell. 2020. Project Bluefire. https://www.waveswell.com/project-bluefire/ (2020-09-10)

[32] Ocean Power Technologies. 2020. Our Company. https://oceanpowertechnologies.com/our-company/ (2020-09-11)

[33] Ocean Power Technologies. 2020. PB3 PowerBuoy. https://oceanpowertechnologies.com/pb3-powerbuoy/ (2020-09-11)

[34] Waara, A. 2015. Vågkraftsanläggning ansluten till svenska kraftnätet. Uppsala University. 17 December. https://www.uppsalauniversitet.se/nyheter-press/nyheter/artikel/?id=5866&typ=artikel&lang=sv (2020-10-16)

[35] Seabased. 2020. Wave Power Parks. https://reed-sunfish-s2ay.squarespace.com/seabased-wave-parks (2020-09-11)

[36] O'Halloran, B. 2013. Ocean energy developer Wavebob set to go under. The Irish Times. 3 April. https://www.irishtimes.com/business/ocean-energy-developer-wavebob-set-to-go-under-1.1347036 (2020-09-18)

[37] AWS Ocean Energy. 2020. Archimedes Waveswing. http://www.awsocean.com/technology.html# (2020-09-11)

[38] Rusu, E. Onea, F. 2018. A review of the technologies for wave energy extraction. *Clean Energy*. 2:1, 10-19.

[39] Falnes, J. N.d. Principles for capture of energy from ocean waves. Phase control and optimum oscillation. http://folk.ntnu.no/falnes/web_arkiv/InstFysikk/phcontrl.pdf (2020-10-20)

[40] Falnes, J. 2002. Ocean Waves and Oscillating Systems: linear interactions including wave-energy extraction. Cambridge: Cambridge University Press.

[41] Hals Todalshaug, J. 2017. Hydrodynamics of WECs. In Pecher Arthur and Kofoed Jens Peter (editors). *Handbook of Ocean Wave Energy*. Volume 7. Springer, 139-158.

[42] Faedo, N. Olaya, S. Ringwood, J V. 2017. Optimal control, MPC, and MPC-like algorithms for wave energy systems: an overview. *IFAC Journal of Systems and Control*. 1, 37-56.

[43] Hals, J. Falnes, J. Moan, T. 2011. Constrained Optimal Control of a Heaving Buoy Wave-Energy Converter. *Journal of Offshore Mechanics and Arctic Engineering*. 133, 011401.

[44] Milani, F. Moghaddam, R K. 2017. Power Maximization of A Point Absorber Wave Energy Converter Using Improved Model Predictive Control. *China Ocean Engineering*. 31:4, 510-516.

[45] Li, G. Belmont, M R. 2014. Model predictive control of sea wave energy converters – Part I: A convex approach for the case of a single device. *Renewable Energy*. 69, 453-463.

[46] Perez, T. Fossen, T I. 2008. Joint Identification of Infinite-Frequency Added Mass and Fluid-memory Models of Marine Structures. *Modeling, Identification and Control*. 29:3, 93-102.

[47] Ljung, L. Glad, T. 2004. *Modellbygge och simulering*. Lund: Studentlitteratur.

[48] MathWorks. 2020. *Simulink® Control Design™ User's Guide*.

[49] Anton, H. Rorres, C. 2011. *Elementary Linear Algebra – with Supplemental Applications.* 10th ed. John Wiley & Sons.

[50] Siemens. 2019. Natural Frequency and Resonance. https://community.sw.siemens.com/s/article/Natural-Frequency-and-Resonance (2020-11-20)

[51] Fish, G. Dempsey, M. Delgado, J G. Roberts, N. 2012. Natural frequency analysis of Modelica powertrain models. In: *Proceedings of the 9th International Modelica Conference.* Münich, Germany, 3-5 September.

Appendix A

Table 3. States and eigenvectors for the eigenvalues $-0.0185 \pm 0.7675i$ and $0.0021 \pm 0.4301i$ as well a demonstration of typical values for these states at the same simulation time. The radiation states for the operating case could not be extracted, therefore, an assumption was made that the radiation block did not have a big impact on the eigenvectors.

State	Operating value at $t_s = 0\ s$	$-0.0185 \pm 0.7675i$	$0.0021 \pm 0.4301i$
PTO - flywheel	-0.0159	-2.904e-08 + 1.2153e-06i	3.07e-09 + 6.8103e-07i
PTO - no freewheel	-7.5853e-07	-9.088e-12 - 2.9022e-13i	-2.8542e-12 + 1.0581e-13i
PTO - V_gear	-0.0159	-2.9035e-08 + 1.2153e-06i	3.1479e-09 + 6.8104e-07i
PTO - E_E1	9.4524e+7	0.71992 + 0i	0.71992 + 0i
PTO - m_E1	457.15	3.3648e-06 - 2.5403e-10i	3.3648e-06 + 5.8503e-11i
PTO - E_E	9.8871e+8	-0.69364 + 5.4626e-07i	-0.69364 - 5.6015e-05i
PTO - m_E	478.18	-3.4777e-06 + 2.2699e-10i	-3.4777e-06 - 4.2145e-10i
PTO - mdot_mainvalve	-0.03512	-2.5565e-10 + 1.062e-08i	2.765e-11 + 5.9518e-09i
PTO - E_FAS	3.2151e+6	0.024169 - 7.0605e-05i	0.024167 - 3.9576e-05i
PTO - m_FAS	15.549	1.1291e-07 + 2.5837e-11i	1.1289e-07 + 3.6207e-10i
Hydro - dist. buoy (surge)	0.03960	-2.4952e-05 + 8.3066e-06i	1.4488e-06 - 1.3144e-05i
Hydro - dist. buoy (sway)	0.01154	-3.0892e-06 + 1.1824e-06i	-7.2557e-06 + 5.4802e-05i
Hydro - dist. buoy (heave)	-0.01018	3.9773e-08 - 4.1218e-09i	2.8763e-08 - 4.436e-09i
Hydro - dist. buoy (roll)	-0.0004413	-6.5882e-07 + 2.16e-07i	7.7337e-08 - 6.3613e-07i
Hydro - dist. buoy (pitch)	0.0016128	-1.6967e-07 + 5.5236e-08i	2.7053e-08 - 2.1745e-07i
Hydro - dist. buoy (yaw)	1.8544e-05	1.5781e-08 - 2.565e-08i	1.7616e-08 + 7.3739e-08i
Hydro - vel. buoy (surge)	-0.03174	-5.9137e-06 - 1.9304e-05i	5.6566e-06 + 5.9533e-07i
Hydro - vel. buoy (sway)	-0.0006451	-8.4626e-07 - 2.3959e-06i	-2.3586e-05 - 2.9992e-06i
Hydro - vel. buoy (heave)	-0.0003013	9.7564e-09 - 2.2961e-09i	-3.4477e-09 + 3.2311e-08i
Hydro - vel. buoy (roll)	0.00034866	-1.536e-07 - 5.0967e-07i	2.7382e-07 + 3.1953e-08i
Hydro - vel. buoy (pitch)	-0.0020270	-3.9266e-08 - 1.3125e-07i	9.3605e-08 + 1.118e-08i
Hydro - vel. buoy (yaw)	5.3592e-06	1.7054e-08 + 1.3289e-08i	-3.1366e-08 + 5.4906e-09i
Hydro - dist. slide (surge)	0.0396639	-2.4911e-05 + 8.2913e-06i	1.4496e-06 - 1.3148e-05i

Hydro - dist. slide (sway)	0.0115596	-3.0501e-06 + 1.1693e-06i	-7.2554e-06 + 5.4803e-05i
Hydro - dist. slide (heave)	5.7123e-06	1.0599e-08 - 4.0938e-09i	-3.3389e-10 - 4.4358e-09i
Hydro - dist. slide (roll)	-0.000440	-6.5831e-07 + 2.1584e-07i	7.7338e-08 - 6.3642e-07i
Hydro - dist. slide (pitch)	0.001596	-1.7015e-07 + 5.5439e-08i	2.705e-08 - 2.1751e-07i
Hydro - dist. slide (yaw)	3.2362e-08	4.6673e-10 - 1.7438e-10i	-9.5859e-11 + 8.8914e-10i
Hydro - vel. slide (surge)	-0.031809	-5.9021e-06 - 1.9273e-05i	5.6584e-06 + 5.9657e-07i
Hydro - vel. slide (sway)	-0.000658	-8.409e-07 - 2.3627e-06i	-2.3587e-05 - 3.0083e-06i
Hydro - vel. slide (heave)	-6.8705e-06	1.043e-08 - 2.4339e-08i	-3.5778e-09 + 1.9791e-08i
Hydro - vel. slide (roll)	0.000345	-1.5346e-07 - 5.0925e-07i	2.739e-07 + 3.1961e-08i
Hydro - vel. slide (pitch)	-0.002012	-3.9397e-08 - 1.3162e-07i	9.3615e-08 + 1.119e-08i
Hydro - vel. slide (yaw)	-6.8997e-07	-2.2052e-09 + 1.0602e-09i	-6.8663e-11 - 2.2701e-09i
Hydro - surge radiation	-	2.1192e-06 + 1.0854e-06i	-1.8598e-07 + 7.0322e-08i
Hydro - surge radiation	-	1.3468e-06 - 2.7937e-06i	1.6142e-07 + 4.3315e-07i
Hydro - surge radiation	-	-3.6803e-06 - 1.666e-06i	1.0088e-06 - 3.7048e-07i
Hydro - surge radiation	-	-2.7751e-09 + 4.6584e-09i	-1.6648e-10 - 5.1972e-10i
Hydro - surge radiation	-	6.1532e-09 + 3.4672e-09i	-1.2101e-09 + 3.8126e-10i
Hydro - surge radiation	-	4.3215e-09 - 8.1215e-09i	8.7296e-10 + 2.8176e-09i
Hydro - surge radiation	-	-1.0711e-08 - 5.372e-09i	6.56e-09 - 1.9982e-09i
Hydro - sway radiation	-	2.7225e-07 + 1.2521e-07i	7.8359e-07 - 2.7707e-07i
Hydro - sway radiation	-	1.5449e-07 - 3.5845e-07i	-6.3545e-07 - 1.8248e-06i
Hydro - sway radiation	-	-4.7162e-07 - 1.8991e-07i	-4.2493e-06 + 1.4571e-06i
Hydro - sway radiation	-	-1.0747e-08 + 1.8122e-08i	-4.9093e-10 - 1.5186e-09i
Hydro - sway radiation	-	2.3936e-08 + 1.3424e-08i	-3.5358e-09 + 1.1245e-09i
Hydro - sway radiation	-	1.6729e-08 - 3.1591e-08i	2.5751e-09 + 8.2326e-09i
Hydro - sway radiation	-	-4.1662e-08 - 2.0791e-08i	1.9168e-08 - 5.8953e-09i
Hydro - heave radiation	-	-1.4707e-09 + 4.2879e-10i	6.8597e-10 - 5.413e-10i
Hydro - heave radiation	-	6.0458e-10 + 1.9016e-09i	-1.2508e-09 - 1.6007e-09i

Hydro - heave radiation	-	2.4572e-09 - 8.4704e-10i	-3.7353e-09 + 2.8902e-09i
Hydro - heave radiation	-	-1.1802e-09 - 3.173e-09i	6.6778e-09 + 8.7158e-09i
Hydro - heave radiation	-	-4.0947e-09 + 1.6366e-09i	2.0337e-08 - 1.5428e-08i
Mooring - flexleg lump vel.	0.002690	-4.2685e-06 - 1.3892e-05i	2.4602e-06 + 2.2441e-07i
Mooring - flexleg lump vel.	0.004032	-3.5877e-06 - 1.1509e-05i	-1.4999e-05 - 1.9697e-06i
Mooring - flexleg lump vel.	-2.8127e-06	1.568e-09 + 4.708e-09i	1.6447e-09 + 1.1333e-10i
Mooring - flexleg lump vel.	0.002093	-3.3976e-06 - 1.1072e-05i	3.2779e-06 + 3.4553e-07i
Mooring - flexleg lump vel.	0.003907	-3.4248e-06 - 1.0966e-05i	-1.6207e-05 - 2.1194e-06i
Mooring - flexleg lump vel.	-2.6246e-06	1.1823e-09 + 3.3491e-09i	1.5317e-09 + 5.4702e-11i
Mooring - flexleg lump vel.	0.001263	-2.8996e-06 - 9.4616e-06i	3.8285e-06 + 4.2526e-07i
Mooring - flexleg lump vel.	0.004051	-3.1919e-06 - 1.0197e-05i	-1.7054e-05 - 2.222e-06i
Mooring - flexleg lump vel.	-2.3007e-06	9.0804e-10 + 2.3517e-09i	1.4423e-09 + 1.3488e-12i
Mooring - flexleg lump vel.	0.000291	-2.7114e-06 - 8.856e-06i	4.229e-06 + 4.7969e-07i
Mooring - flexleg lump vel.	0.004142	-2.9893e-06 - 9.5279e-06i	-1.7771e-05 - 2.3089e-06i
Mooring - flexleg lump vel.	-1.8049e-06	7.6571e-10 + 1.7828e-09i	1.3814e-09 - 4.5693e-11i
Mooring - flexleg lump vel.	-0.001249	-2.7745e-06 - 9.0657e-06i	4.5246e-06 + 5.1573e-07i
Mooring - flexleg lump vel.	0.003980	-2.8344e-06 - 9.0127e-06i	-1.8428e-05 - 2.3893e-06i
Mooring - flexleg lump vel.	-7.1147e-07	7.6619e-10 + 1.6774e-09i	1.353e-09 - 8.5687e-11i
Mooring - flexleg lump vel.	-0.002613	-3.0366e-06 - 9.9213e-06i	4.7262e-06 + 5.3583e-07i
Mooring - flexleg lump vel.	0.003918	-2.7153e-06 - 8.6135e-06i	-1.9027e-05 - 2.463e-06i
Mooring - flexleg lump vel.	3.3416e-07	9.123e-10 + 2.0445e-09i	1.3627e-09 - 1.1785e-10i
Mooring - flexleg lump vel.	-0.004532	-3.4617e-06 - 1.1305e-05i	4.8415e-06 + 5.4169e-07i
Mooring - flexleg lump vel.	0.003752	-2.6217e-06 - 8.2968e-06i	-1.9566e-05 - 2.5298e-06i
Mooring - flexleg lump vel.	2.0784e-06	1.2097e-09 + 2.9022e-09i	1.4178e-09 - 1.4118e-10i
Mooring - flexleg lump vel.	-0.006580	-4.0248e-06 - 1.3137e-05i	4.8744e-06 + 5.3432e-07i
Mooring - flexleg lump vel.	0.003517	-2.5439e-06 - 8.0311e-06i	-2.0041e-05 - 2.5888e-06i
Mooring - flexleg lump vel.	4.1740e-06	1.6664e-09 + 4.2765e-09i	1.526e-09 - 1.545e-10i

Mooring - flexleg lump vel.	-0.008605	-4.7084e-06 - 1.5358e-05i	4.8279e-06 + 5.1442e-07i
Mooring - flexleg lump vel.	0.003173	-2.4741e-06 - 7.7908e-06i	-2.045e-05 - 2.6398e-06i
Mooring - flexleg lump vel.	6.4994e-06	2.2935e-09 + 6.203e-09i	1.6974e-09 - 1.5629e-10i
Mooring - flexleg lump pos.	0.01105	-1.7956e-05 + 5.995e-06i	5.4897e-07 - 5.717e-06i
Mooring - flexleg lump pos.	0.003475	-1.4874e-05 + 5.0336e-06i	-4.7455e-06 + 3.4847e-05i
Mooring - flexleg lump pos.	-23.6949	6.0814e-09 - 2.1898e-09i	2.8169e-10 - 3.8223e-09i
Mooring - flexleg lump pos.	0.012005	-1.4311e-05 + 4.7722e-06i	8.3961e-07 - 7.6166e-06i
Mooring - flexleg lump pos.	0.00376	-1.4172e-05 + 4.8043e-06i	-5.1069e-06 + 3.7655e-05i
Mooring - flexleg lump pos.	-22.1949	4.3239e-09 - 1.6449e-09i	1.4414e-10 - 3.5603e-09i
Mooring - flexleg lump pos.	0.013019	-1.2229e-05 + 4.0732e-06i	1.0311e-06 - 8.8958e-06i
Mooring - flexleg lump pos.	0.004071	-1.3178e-05 + 4.4769e-06i	-5.3548e-06 + 3.9623e-05i
Mooring - flexleg lump pos.	-20.6949	3.0338e-09 - 1.2563e-09i	1.9117e-11 - 3.3532e-09i
Mooring - flexleg lump pos.	0.01412	-1.1447e-05 + 3.8091e-06i	1.162e-06 - 9.8263e-06i
Mooring - flexleg lump pos.	0.0044019	-1.2313e-05 + 4.1921e-06i	-5.5647e-06 + 4.1288e-05i
Mooring - flexleg lump pos.	-19.1949	2.2975e-09 - 1.0531e-09i	-9.092e-11 - 3.2121e-09i
Mooring - flexleg lump pos.	0.01533	-1.1718e-05 + 3.8978e-06i	1.2491e-06 - 1.0513e-05i
Mooring - flexleg lump pos.	0.004760	-1.1647e-05 + 3.9741e-06i	-5.7588e-06 + 4.2816e-05i
Mooring - flexleg lump pos.	-17.6949	2.1602e-09 - 1.0504e-09i	-1.8421e-10 - 3.1464e-09i
Mooring - flexleg lump pos.	0.01666	-1.2824e-05 + 4.266e-06i	1.2981e-06 - 1.0982e-05i
Mooring - flexleg lump pos.	0.005149	-1.1131e-05 + 3.8065e-06i	-5.9369e-06 + 4.4207e-05i
Mooring - flexleg lump pos.	-16.1949	2.6336e-09 - 1.2522e-09i	-2.5889e-10 - 3.1694e-09i
Mooring - flexleg lump pos.	0.01812	-1.4613e-05 + 4.863e-06i	1.313e-06 - 1.125e-05i
Mooring - flexleg lump pos.	0.005572	-1.0721e-05 + 3.6747e-06i	-6.0981e-06 + 4.5459e-05i
Mooring - flexleg lump pos.	-14.6949	3.7411e-09 - 1.6664e-09i	-3.1251e-10 - 3.2976e-09i
Mooring - flexleg lump pos.	0.01972	-1.698e-05 + 5.6538e-06i	1.2962e-06 - 1.1326e-05i
Mooring - flexleg lump pos.	0.006030	-1.0378e-05 + 3.5651e-06i	-6.2405e-06 + 4.6562e-05i
Mooring - flexleg lump pos.	-13.1949	5.5164e-09 - 2.3043e-09i	-3.4226e-10 - 3.5493e-09i

Mooring - flexleg lump pos.	0.02147	-1.9851e-05 + 6.6139e-06i	1.2494e-06 - 1.1218e-05i
Mooring - flexleg lump pos.	0.006527	-1.0067e-05 + 3.4665e-06i	-6.3636e-06 + 4.7514e-05i
Mooring - flexleg lump pos.	-11.6949	8.0053e-09 - 3.1814e-09i	-3.4454e-10 - 3.9479e-09i
Mooring - flexleg lump torsion ang. vel.	-9.7133e-05	1.2098e-10 + 3.4927e-10i	-3.6983e-10 - 3.8089e-11i
Mooring - flexleg lump torsion ang. vel.	0.000185	1.1679e-10 + 3.3715e-10i	-3.5705e-10 - 3.6773e-11i
Mooring - flexleg lump torsion ang. vel.	-0.000254	1.126e-10 + 3.2503e-10i	-3.4427e-10 - 3.5457e-11i
Mooring - flexleg lump torsion ang. vel.	0.000298	1.084e-10 + 3.1291e-10i	-3.3148e-10 - 3.414e-11i
Mooring - flexleg lump torsion ang. vel.	-0.000312	1.0421e-10 + 3.0078e-10i	-3.187e-10 - 3.2824e-11i
Mooring - flexleg lump torsion ang. vel.	0.000295	1.0002e-10 + 2.8866e-10i	-3.0592e-10 - 3.1508e-11i
Mooring - flexleg lump torsion ang. vel.	-0.000249	9.5828e-11 + 2.7654e-10i	-2.9314e-10 - 3.0192e-11i
Mooring - flexleg lump torsion ang. vel.	0.000178	9.1636e-11 + 2.6442e-10i	-2.8036e-10 - 2.8876e-11i
Mooring - flexleg lump torsion ang. Vel.	-8.9223e-05	8.7444e-11 + 2.523e-10i	-2.6757e-10 - 2.756e-11i
Mooring - flexleg lump torsion angle	2.2004e-08	4.51e-10 - 1.6852e-10i	-9.2647e-11 + 8.5936e-10i
Mooring - flexleg lump torsion angle	4.7784e-08	4.3535e-10 - 1.6268e-10i	-8.9446e-11 + 8.2966e-10i
Mooring - flexleg lump torsion angle	4.7284e-09	4.197e-10 - 1.5684e-10i	-8.6245e-11 + 7.9996e-10i
Mooring - flexleg lump torsion angle	5.6794e-08	4.0405e-10 - 1.51e-10i	-8.3044e-11 + 7.7026e-10i
Mooring - flexleg lump torsion angle	-3.6443e-09	3.884e-10 - 1.4516e-10i	-7.9842e-11 + 7.4056e-10i
Mooring - flexleg lump torsion angle	5.5271e-08	3.7275e-10 - 1.3932e-10i	-7.6641e-11 + 7.1086e-10i
Mooring - flexleg lump torsion angle	-8.4422e-10	3.5709e-10 - 1.3348e-10i	-7.344e-11 + 6.8116e-10i
Mooring - flexleg lump torsion angle	4.2977e-08	3.4144e-10 - 1.2764e-10i	-7.0239e-11 + 6.5145e-10i
Mooring - flexleg lump torsion angle	1.1314e-08	3.2579e-10 - 1.218e-10i	-6.7037e-11 + 6.2175e-10i
Mooring - line 1 lump vel.	0.000696	2.6685e-06 + 8.6783e-06i	-9.5585e-07 - 6.6685e-08i
Mooring - line 1	0.000754	2.3551e-06 + 7.5587e-06i	9.6263e-06 + 1.2652e-06i

lump vel.			
Mooring - line 1 lump vel.	-6.0161e-07	-1.0695e-09 - 3.5146e-09i	-1.3083e-09 - 2.0517e-10i
Mooring - line 1 lump vel.	0.001317	2.6924e-06 + 8.7564e-06i	-1.0677e-06 - 8.0371e-08i
Mooring - line 1 lump vel.	0.001547	2.4262e-06 + 7.7845e-06i	1.0111e-05 + 1.3279e-06i
Mooring - line 1 lump vel.	-1.1703e-06	-1.0862e-09 - 3.6208e-09i	-1.3609e-09 - 2.3014e-10i
Mooring - line 1 lump vel.	0.001898	2.0023e-08 + 6.816e-08i	-4.2913e-07 - 5.3923e-08i
Mooring - line 1 lump vel.	0.002247	8.8562e-08 + 2.7249e-07i	1.4681e-06 + 1.8751e-07i
Mooring - line 1 lump vel.	-1.7035e-06	-1.3637e-11 - 2.0054e-10i	-1.4078e-10 - 7.2061e-11i
Mooring - line 1 lump vel.	0.002568	-2.7479e-06 - 8.9336e-06i	6.0269e-07 + 2.0345e-08i
Mooring - line 1 lump vel.	0.003050	-2.3504e-06 - 7.5564e-06i	-8.378e-06 - 1.1072e-06i
Mooring - line 1 lump vel.	-2.3009e-06	1.1029e-09 + 3.3616e-09i	1.168e-09 + 9.8132e-11i
Mooring - line 1 lump pos.	0.002030	1.1217e-05 - 3.7476e-06i	-1.6562e-07 + 2.2214e-06i
Mooring - line 1 lump pos.	0.000639	9.7687e-06 - 3.3043e-06i	3.048e-06 - 2.2365e-05i
Mooring - line 1 lump pos.	-40.438	-4.543e-09 + 1.5031e-09i	-4.9147e-10 + 3.0394e-09i
Mooring - line 1 lump pos.	0.004060	1.1318e-05 - 3.7812e-06i	-1.9868e-07 + 2.4813e-06i
Mooring - line 1 lump pos.	0.001278	1.0061e-05 - 3.4039e-06i	3.1992e-06 - 2.3491e-05i
Mooring - line 1 lump pos.	-36.6279	-4.6808e-09 + 1.5282e-09i	-5.5011e-10 + 3.1612e-09i
Mooring - line 1 lump pos.	0.006090	8.8126e-08 - 2.8216e-08i	-1.3012e-07 + 9.9705e-07i
Mooring - line 1 lump pos.	0.001917	3.5204e-07 - 1.2389e-07i	4.522e-07 - 3.4111e-06i
Mooring - line 1 lump pos.	-32.8169	-2.6071e-10 + 2.4061e-11i	-1.6909e-10 + 3.2648e-10i
Mooring - line 1 lump pos.	0.008120	-1.1547e-05 + 3.8591e-06i	5.3976e-08 - 1.4009e-06i
Mooring - line 1 lump pos.	0.002557	-9.7659e-06 + 3.2981e-06i	-2.6668e-06 + 1.9465e-05i
Mooring - line 1 lump pos.	-29.0059	4.3428e-09 - 1.5419e-09i	2.4108e-10 - 2.7144e-09i
Mooring - line 1 lump torsion ang. vel.	7.1511e-07	6.6671e-11 + 1.9246e-10i	-2.0317e-10 - 2.0876e-11i
Mooring - line 1 lump torsion ang. vel.	7.2186e-08	5.0003e-11 + 1.4435e-10i	-1.5238e-10 - 1.5657e-11i
Mooring - line 1 lump torsion ang. vel.	5.1484e-08	3.3336e-11 + 9.6232e-11i	-1.0159e-10 - 1.0438e-11i

Mooring - line 1 lump torsion ang. vel.	2.5934e-08	1.6668e-11 + 4.8116e-11i	-5.0793e-11 - 5.2188e-12i
Mooring - line 1 lump torsion angle	1.7153e-08	2.4853e-10 - 9.2866e-11i	-5.0784e-11 + 4.7211e-10i
Mooring - line 1 lump torsion angle	1.2881e-08	1.8639e-10 - 6.965e-11i	-3.8088e-11 + 3.5408e-10i
Mooring - line 1 lump torsion angle	8.5890e-09	1.2426e-10 - 4.6433e-11i	-2.5392e-11 + 2.3605e-10i
Mooring - line 1 lump torsion angle	4.2950e-09	6.2132e-11 - 2.3217e-11i	-1.2696e-11 + 1.1803e-10i
Mooring - mooring buoy dist. (surge)	0.0101	-2.3574e-05 + 7.8791e-06i	1.1222e-07 - 2.8748e-06i
Mooring - mooring buoy dist. (sway)	0.003196	-1.4449e-05 + 4.8827e-06i	-4.1452e-06 + 3.0316e-05i
Mooring - mooring buoy dist. (heave)	-25.1949	8.2165e-09 - 2.861e-09i	4.2136e-10 - 4.0675e-09i
Mooring - mooring buoy dist. (roll)	-0.000176	6.8597e-07 - 2.3413e-07i	3.5425e-07 - 2.637e-06i
Mooring - mooring buoy dist. (pitch)	0.000567	6.8606e-07 - 2.3416e-07i	3.5433e-07 - 2.6376e-06i
Mooring - mooring buoy dist. (yaw)	2.3612e-08	3.1011e-10 - 1.1595e-10i	-6.386e-11 + 5.9218e-10i
Mooring - mooring buoy vel. (surge)	0.003311	-5.6105e-06 - 1.8239e-05i	1.2368e-06 + 4.2378e-08i
Mooring - mooring buoy vel. (sway)	0.003818	-3.4798e-06 - 1.118e-05i	-1.3048e-05 - 1.7208e-06i
Mooring - mooring buoy vel. (heave)	-3.7345e-07	-1.9254e-08 + 5.0855e-09i	-9.8602e-09 + 7.2603e-08i
Mooring - mooring buoy vel. (roll)	-0.000226	1.6698e-07 + 5.3082e-07i	1.135e-06 + 1.4699e-07i
Mooring - mooring buoy vel. (pitch)	-0.000342	1.6701e-07 + 5.3089e-07i	1.1353e-06 + 1.4698e-07i
Mooring - mooring buoy vel. (yaw)	-8.5093e-06	1.1073e-09 - 8.5733e-12i	4.5381e-10 - 3.8276e-09i